Rheology of the Lower Crust and Upper Mantle: Evidence from Rock Mechanics, Geodesy, and Field Observations

Roland Bürgmann[1] and Georg Dresen[2]

[1]Department of Earth and Planetary Science, University of California, Berkeley, California 94720; email: burgmann@seismo.berkeley.edu

[2]GeoForschungsZentrum Potsdam, D-14473 Potsdam, Germany; email: dre@gfz-potsdam.de

Annu. Rev. Earth Planet. Sci. 2008. 36:531–67

First published online as a Review in Advance on February 12, 2008

The *Annual Review of Earth and Planetary Sciences* is online at earth.annualreviews.org

This article's doi:
10.1146/annurev.earth.36.031207.124326

0084-6597/08/0530-0531$20.00

Key Words

brittle-ductile transition, deformation mechanisms, postseismic relaxation, shear zones, viscosity

Abstract

Rock-mechanics experiments, geodetic observations of postloading strain transients, and micro- and macrostructural studies of exhumed ductile shear zones provide complementary views of the style and rheology of deformation deep in Earth's crust and upper mantle. Overall, results obtained in small-scale laboratory experiments provide robust constraints on deformation mechanisms and viscosities at the natural laboratory conditions. Geodetic inferences of the viscous strength of the upper mantle are consistent with flow of mantle rocks at temperatures and water contents determined from surface heat-flow, seismic, and mantle xenolith studies. Laboratory results show that deformation mechanisms and rheology strongly vary as a function of stress, grain size, and fluids. Field studies reveal a strong tendency for deformation in the lower crust and uppermost mantle in and adjacent to fault zones to localize into systems of discrete shear zones with strongly reduced grain size and strength. Deformation mechanisms and rheology may vary over short spatial (shear zone) and temporal (earthquake cycle) scales.

INTRODUCTION

Lithosphere: the strong outer layer of Earth that comprises mobile tectonic plates and includes both the crust and uppermost mantle; heat is transferred conductively

Asthenosphere: weak and ductile upper-mantle layer below the lithosphere; heat is transported convectively

The deformation of rocks in response to forces in Earth's interior is governed by rock rheology. Rheology is "the study of the flow and deformation of all forms of matter" [the term and definition were coined in 1929 by E.C. Bingham, inspired by a quote from Heraclitus, "panta rhei—everything flows" (Reiner 1964)]. As such, rheology is concerned with describing material properties through constitutive equations that relate stress and strain rate. We often use the term rheology when referring to such constitutive relations.

Knowledge of rock rheology is fundamental to understanding the evolution and dynamics of Earth and other planets. The occurrence and nature of plate tectonics are prescribed by the relative strength and mobility of lithospheric plates over weaker, underlying asthenospheric mantle and on the localization of deformation along relatively narrow plate boundary zones. Plate tectonics appears unique to Earth in our planetary system, and the expression of tectonics on other planetary bodies must be closely tied to differences in the rheology of their interiors. Since the advent of plate tectonics, we have come to realize that understanding the kinematics of moving plates is insufficient to fully describe how Earth's lithosphere interacts with mantle convection and various driving forces. This is evident when considering the complex deformation patterns of broadly distributed plate boundary zones, which can now be mapped with great precision using space geodetic methods. Localized and often episodic deformation (the earthquake cycle) in the brittle upper crust is coupled to viscous flow in Earth's lower crust and upper mantle. Thus, the rheology of viscously deforming rocks at depth is of fundamental importance when trying to understand the time-dependent deformation and hazard along active fault zones.

Assessing the mechanical properties of rocks for the broad range of thermodynamic boundary conditions prevalent in Earth's interior remains a daunting task. Rock rheology varies as a function of a number of constitutive and environmental aspects, including mineralogy, fluid content and chemistry, mineral grain size, melt fraction, temperature, pressure, and differential stress conditions. The range in mineralogical and chemical composition of rocks is enormous, and our knowledge of even the most important boundary conditions, such as regional heat flow and tectonic forces, is often rudimentary. Relevant timescales range from fractions of a second during dynamic earthquake rupture to millions of years in the formation of mountain chains or sedimentary basins. Length scales pertinent to deformation processes range from crystal lattice spacing to the width of orogenic plateaus.

Jelly Sandwich, Crème Brûlée, and Banana Split: A Gourmet Perspective of Lithospheric Strength

We can use a diverse menu of food analogies to describe varying views of the distribution of rheological properties and strength in Earth. Increasing pressure and temperature and the compositional layering of continental crust result in strong rheological

layering. Earth's upper crust is thought to be in a state of frictional equilibrium with active faults limiting strength, consistent with Mohr-Coulomb theory and friction coefficients (f) of 0.6–1.0 as derived from laboratory experiments [often referred to as Byerlee's law (Byerlee 1978)]. The pressure-dependent increase of the frictional strength of rocks with depth is ultimately bound by thermally activated creep processes reducing viscous strength with increasing temperature and depth (e.g., Brace & Kohlstedt 1980, Goetze & Evans 1979). Across this brittle-ductile transition, the deformation mode and dominant deformation mechanisms operating in continental rocks gradually change over a broad range of temperatures between approximately 300°C and 500°C. More mafic rock types, and generally rocks with higher melting temperatures, have higher viscosities at a given temperature. Resulting profiles for continental lithosphere constitute the now classic strength paradigm with a weak middle and lower crust sandwiched between strong upper crust and strong mantle lithosphere, appropriately dubbed the jelly sandwich model (**Figure 1*a***). In this model, much of the long-term strength of tectonic plates lies in the lithospheric mantle.

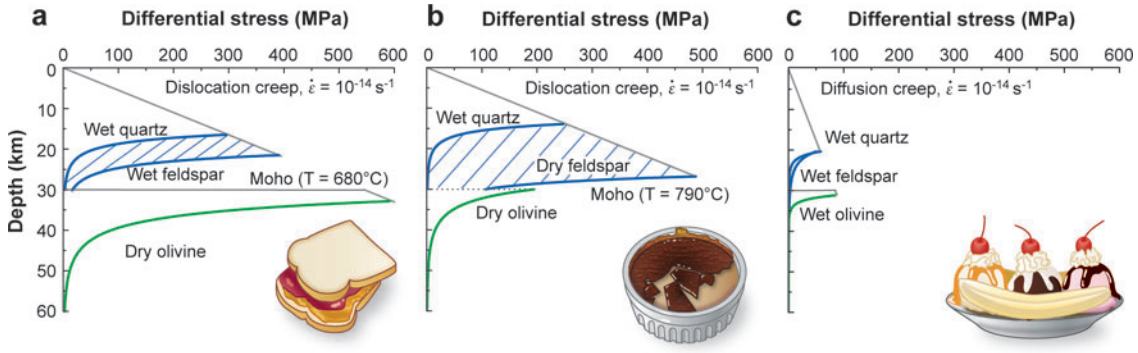

Figure 1

Schematic view of alternative first-order models of strength through continental lithosphere. In the upper crust, frictional strength increases with pressure and depth. In the two left panels a coefficient of friction following Byerlee's law and hydrostatic fluid pressure (ratio of pore pressure to lithostatic pressure $\lambda = 0.4$) are assumed in a strike-slip tectonic regime. In the right panel, low friction due to high pore fluid pressure ($\lambda = 0.9$) is assumed. (*a*) A jelly sandwich strength envelope is characterized by a weak mid-to-lower crust and a strong mantle composed dominantly of dry olivine (Hirth & Kohlstedt 2003). (*b*) The crème brûlée model posits that the mantle is weak (in the case shown resulting from a higher geotherm, adding water would produce a dramatic further strength reduction). The dry and brittle crust defines the strength of the lithosphere. (*c*) The banana split model considers the weakness of major crustal fault zones throughout the thickness of the lithosphere, caused by various strain weakening and feedback processes. Owing to small grain size in shear zones, deformation in the lower crust and upper mantle is assumed to be accommodated by linear diffusion creep (grain size of 50 μm). Strength envelopes are based on flow law parameters presented in **Supplemental Table 1**. For the crust, a quartz and feldspar rheology was used (Rutter & Brodie 2004a,b; Rybacki et al. 2006). We assumed a geothermal gradient corresponding to surface heat flow of 80 mW m^{-2} (90 mW m^{-2} for the crème brûlée model to avoid overly strong, dry lower crust) and a uniform strain rate of 10^{-14} s^{-1}.

In striking contrast to the jelly sandwich model, some researchers have suggested that the strength of continental lithosphere resides entirely in the crust and that the upper mantle is significantly weaker owing to high temperature and weakening by water (Jackson 2002) (**Figure 1*b***). Proponents of this model, later termed the crème brûlée model by Burov & Watts (2006), also infer a close correlation between the thickness of the seismogenic layer and estimates of the elastic thickness of the continental lithosphere. However, regional estimates of continental elastic thickness from gravity data vary significantly and do not necessarily preclude a strong mantle layer (Burov & Watts 2006).

Finally, some have argued that the strength of the lithosphere is greatly reduced along plate boundaries owing to various weakening processes involving thermal, fluid, and strain-rate effects. To stay with the culinary theme, we refer to such lateral strength reduction as the banana split model (**Figure 1*c***). Relative weakness of major fault zones may exist at all depth levels. Although a Byerlee-law strength profile in the upper crust matches observations in continental interiors (Brudy et al. 1997), stress orientations, heat flow, and seismic observations have been interpreted by some to suggest that the San Andreas transform fault in California and other mature fault zones are frictionally very weak ($f < 0.2$) (Zoback et al. 1987). In the viscous regime, shear heating, grain-size reduction, dynamic recrystallization, chemical alterations and phase changes, and the development of rock fabrics can lead to the formation of weakened shear zones. It continues to be a question of much debate as to whether the overall style of continental deformation is governed by the properties and activity of discrete, weakened shear zones or by the bulk rheological properties of the viscously deforming lower lithosphere.

Uncertainty about the degree of localization at depth below active fault zones is also reflected in an ongoing debate of the first-order nature of earthquake-cycle deformation, with end-member models of the relevant deformation process at depth being either distributed viscous flow or frictional aseismic faulting (Thatcher 1983, Tse & Rice 1986). Ultimately, the distribution of deformation and strength in Earth's outer layers is likely to vary with the tectonic environment, lithology, temperature, availability of fluid, and time, which all contribute to the varied cuisine of continental rheology.

Here, we focus on complementary insights gained from laboratory rock-mechanics experiments, geodetic measurements, and field studies of exhumed deep shear zones. The introduction of new laboratory and analytical techniques in the past decade yielded significant progress in establishing robust constitutive laws that describe the mechanical behavior of major silicate rocks. We complement the view from the rock-mechanics laboratory with information about rheology that can be gleaned from the natural laboratory. Geodetic studies of transient Earth deformation in response to changes in stress from large earthquakes and glacial or lake loads allow for estimates of rheological parameters of rocks at depth. Geological field studies of exhumed deformation zones provide equally important and complementary information about the makeup, environment, and constitutive properties of rocks at depth.

RHEOLOGY: CONSTITUTIVE LAWS AND FORMALISMS

The quantitative description of rheology requires constitutive equations relating stress to strain or strain rates. We can use such equations or flow laws to interpret experimental results, geodetic measurements, and field observations, and their parameters are often empirically derived from such data. Mathematical models of deformation for earthquake-cycle or geodynamic studies rely on appropriate representations of the constitutive properties provided by these equations. Here we provide a brief overview of the most important of these formalisms.

The rheology of the upper crust appears well described by linear elastic relations between stress and strain (Hooke solid, which is represented by a spring in **Figure 2**) at stresses lower than those required to induce brittle fracture of intact rock or frictional sliding of faults. Deformation at higher temperatures and pressures involves both elastic (at short timescales) and viscous behavior. Basic viscoelastic stress-strain relations can be represented by equations that consider various combinations of linear elastic (spring) and linear viscous (dashpot, representing a Newtonian fluid) elements (**Figure 2**). Two commonly utilized linear viscoelastic relations are the Maxwell and Burgers bodies (**Figure 2**). These relations are purely phenomenological representations and are not tied to the actual physical mechanisms accommodating plastic flow at depth. Maxwell materials have an immediate elastic response, but ultimately behave as linear Newtonian fluids. The constitutive equation for deformation of a Maxwell fluid is the sum of the viscous and elastic responses. In shear, $\dot{\varepsilon} = \frac{\dot{\sigma}}{\mu_1} + \frac{\sigma}{\eta_1}$, where $\dot{\varepsilon}$ is engineering shear strain (twice the tensor shear strain rate); σ represents stress (dotted for rates); and μ_1 and η_1 are the shear modulus and viscosity, respectively (**Figure 2**). In response to a stress step $\sigma_0 = \mu_1 \varepsilon_0$, the Maxwell element relaxes exponentially as $\sigma = \mu_1 \varepsilon_0 e^{-\frac{\mu_1}{\eta_1} t}$ with a characteristic relaxation time of $\tau_1 = \frac{\eta_1}{\mu_1}$. The biviscous Burgers body, consisting of a Maxwell fluid and a Kelvin solid (exhibiting a viscously damped elastic response) assembled in series (**Figure 2**), can be used to represent material responses with more than one relaxation time, such as might be

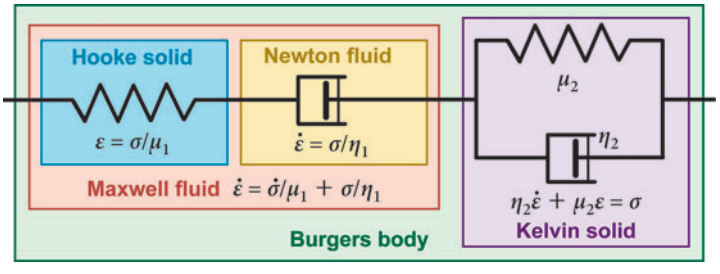

Figure 2

Viscoelastic rheologies can be graphically described by assemblies of springs and dashpots representing linear elastic (Hooke solid) and linear viscous (Newtonian fluid) elements. These elements and the equations they represent form idealized constitutive relationships that are the basis of most geodynamic, tectonic, and earthquake-cycle deformation models. Each named box represents one of the constitutive relations described in the text, which are commonly employed to represent deformation in Earth.

expected for a material with weak inclusions, transient creep, or a nonlinear flow law (Pollitz 2003). The Burgers body exhibits early Kelvin solid behavior and a long-term Maxwell-fluid response described by $\eta_2\ddot{\varepsilon} + \mu_2\dot{\varepsilon} = \frac{\eta_2}{\mu_1}\ddot{\sigma} + [1 + \frac{\mu_2}{\mu_1} + \frac{\eta_2}{\eta_1}]\dot{\sigma} + \frac{\mu_2}{\eta_1}\sigma$, where the relaxation time of the transient Kelvin response $\tau_2 = \frac{\eta_2}{\mu_2}$ is taken to be much shorter than the steady-state relaxation time τ_1. The time dependence of a relaxing Burgers body is well fit by a logarithmic function (Hetland & Hager 2006). We can extend the differential equations describing these time-dependent, viscoelastic material responses to three-dimensional tensor expressions and derive solutions analytically or numerically to explore Earth deformation problems.

Higher-level constitutive relations have been empirically derived from laboratory results, informed by underlying physical principles. The plastic flow of rocks at elevated temperatures ($>\sim 0.5\ T_m$, where T_m is the melting point) is made possible by the thermally activated motion of point, line, and planar mineral-lattice defects. Plastic strain is accommodated by diffusion of ions and vacancies through the crystal lattice and along grain boundaries, grain boundary sliding, and dislocation glide and climb, each of which results in different stress-strain relations. Deformation may also involve solution-precipitation processes with ions transported through a liquid phase such as melt or an H_2O-rich fluid. Steady-state deformation at constant stress may occur when the rate of recovery and recrystallization processes compensate the deformation-induced introduction of crystal defects.

The deformation mechanisms operating in a rock that determine the constitutive behavior depend on phase content, chemical composition, and various thermodynamic variables. Experimental data from a wide range of conditions are well fit with constitutive equations of the form $\dot{\varepsilon} = A\sigma^n d^{-m} f_{H_2O}^r e^{-\frac{(Q+pV)}{RT}}$, where A is a material constant, σ is the stress, n is the (power-law) stress exponent, Q is the activation energy, p is the pressure, V is the activation volume, T is the absolute temperature, R is the molar gas constant, d is the grain size, m is the grain-size exponent, f_{H_2O} is the water fugacity, and r is the fugacity exponent. Diffusion-controlled deformation is linear in stress with $n = 1$ (i.e., flow is linear viscous or Newtonian). Different inverse dependencies on grain size are predicted for lattice diffusion– and grain boundary diffusion–controlled creep with $m = 2$ and $m = 3$, respectively. Creep of fine-grained materials involves grain boundary sliding, which may be controlled by grain boundary diffusion ($n = 1$) or by dislocation motion ($n = 2$). For climb-controlled dislocation creep, deformation is commonly assumed to be grain-size insensitive ($m = 0$) with a stress exponent of $n = 3$–6. We refer to materials for which strain rate is proportional to stress raised to a power $n > 1$ as having a power-law rheology, whose effective viscosity ($\eta = \sigma/\dot{\varepsilon}$) decreases when stress increases. We discuss rigorously determined flow-law parameters for important crustal and mantle materials in the next section and provide these parameters in **Supplemental Table 1** (follow the Supplemental Material link from the Annual Reviews home page at **http://www.annualreviews.org**).

Because the high-temperature deformation mechanisms operate in parallel, strain rates due to their respective contributions add at given stress $\dot{\varepsilon}_{total} = \dot{\varepsilon}_1 + \dot{\varepsilon}_2 + \ldots$. The fastest mechanism is expected to dominate the bulk creep behavior. Thermodynamic

variables including stress and temperature and parameters such as melt content, water content, and grain size determine which mechanism dominates. For example, at low stresses, diffusion-controlled deformation is expected to dominate creep of fine-grained rocks. At elevated stresses and larger grain size, dislocation creep is more important. One can construct deformation mechanism maps that illustrate the primary mechanism and appropriate flow law as a function of these variables (**Figure 3**). The recognition of such variable deformation regimes and their sensitivity to a range of variables poses a significant challenge to the extrapolation of laboratory results to Earth.

The strength of Earth's brittle upper crust is commonly described with the empirical Byerlee's law (Byerlee 1978). The friction coefficient $f = \sigma_s/\sigma_n$ for most rock types ranges from 0.6 to 1. Laboratory experiments show that the shear stress supported by a frictional surface is actually a (logarithmic) function of the fault slip rate and of one or more state variables characterizing the state of asperity contacts: $\sigma_s = \sigma_n[f_0 + a\ln(\frac{v}{v_0}) + b\ln(\frac{v_0\theta}{D_c})]$ where σ_s and σ_n denote shear and normal stress on a fault at failure, f_0 is the friction coefficient at a steady-state slip rate of v_0, v is the frictional slip rate, θ is a state variable that evolves with time, D_c is a critical slip distance, and a and b are empirical constants. Researchers have widely applied these empirically derived rate- and state-dependent friction laws (reviewed in Marone 1998) to describe the mechanics of faulting both at shallow levels and deep in the crust. If friction decreases with sliding velocity ($a - b < 0$, velocity weakening), a fault can undergo spontaneous rupture under appropriate conditions. A velocity-strengthening ($a - b > 0$) fault-zone rheology allows for aseismic fault slip. The finding that faults become velocity strengthening at mid-crustal temperatures suggests that the base of the seismogenic zone could represent a transition to stable sliding, rather than a transition to more distributed ductile flow (Blanpied et al. 1995, Tse & Rice 1986).

VIEW FROM THE LAB

Laboratory experiments probe the physical processes underlying the rheological behavior of rocks and allow us to formulate and test constitutive laws that may be extrapolated with some confidence to conditions in Earth. The extrapolation of laboratory data raises questions about the temporal and spatial scales of deformation, which differ by several orders of magnitude between laboratory and nature. For example, typical strain rates of 10^{-4} to 10^{-6} s^{-1} achieved in high-temperature deformation experiments on centimeter-sized specimens compare with strain-rate estimates of 10^{-9} to 10^{-13} s^{-1} in natural shear zones. Differences in stress, strain rate, finite strain, structural evolution, and thermodynamic conditions (pressure, temperature, fluid fugacity) affect extrapolation of flow laws derived from laboratory experiments. Consequently, predictions of the mechanical behavior and microstructural response at geological conditions have to be tested by geological and geophysical field data, which is the subject of the following two sections.

In recent years, significant progress in experimental work has been achieved by the now common strategy of fabricating synthetic rocks that allow for control of

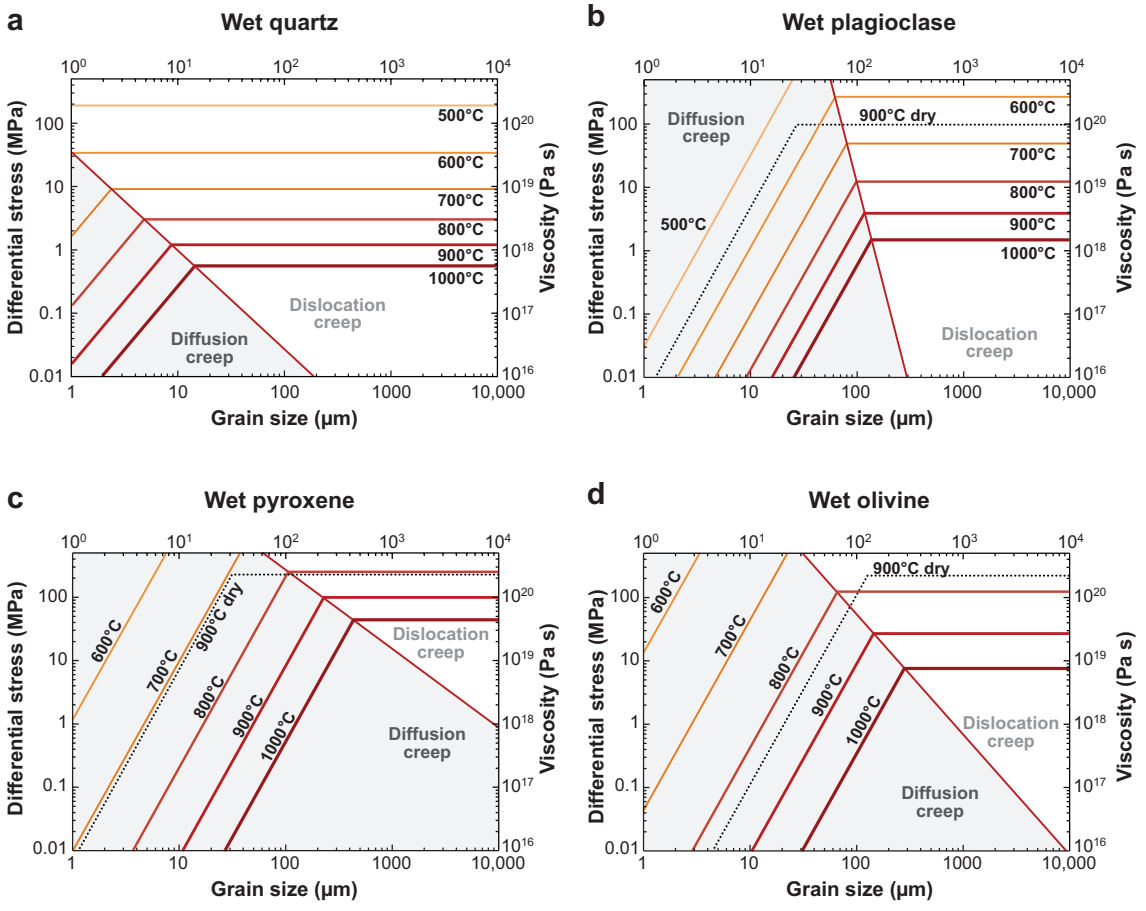

Figure 3

Deformation mechanism maps for wet (nominally saturated in water) rheologies of (*a*) quartz (Rutter & Brodie 2004a,b), (*b*) feldspar (Rybacki et al. 2006), (*c*) pyroxene [wet (Dimanov & Dresen 2005), dry (Bystricky & Mackwell 2001)] and (*d*) olivine (Hirth & Kohlstedt 2003). For construction of the maps, a strain rate of 10^{-12} s^{-1}, a geotherm corresponding to a heat flow of 80 mW m^{-2}, and a rock density of 2.8 g cm^{-3} were assumed. For these conditions, diffusion-controlled creep dominates in rocks with a grain size smaller than ~200 μm at temperatures of approximately 500°C to 900°C except for quartz. For comparison, a dotted line shows the anhydrous relationship at 900°C. Viscosity estimates from geodetic measurements between 1×10^{18} and 10×10^{19} Pa s are in good agreement with the rheology of rocks containing at least trace amounts of H_2O, but not with dry rocks.

important parameters such as grain size, water and impurity content, melt fraction, and mineral phase content. Aided by a new generation of high-temperature deformation apparatuses (Paterson-type) with much improved stress resolution and the capability to achieve large strains, researchers can now constrain a broader range of deformation mechanisms operating in silicates and more precise flow-law parameters

in the laboratory. Here, we briefly review the results of recent laboratory analyses of the rheological behavior of materials that may be considered representative of the lower crust and upper mantle, and for which constitutive equations exist that describe flow in the diffusion and dislocation creep fields. These studies followed similar experimental strategies, facilitating a direct comparison of the rheological behavior. Most experiments used similar high-resolution gas deformation apparatuses under well-defined thermodynamic conditions and include detailed characterization of the starting materials with regard to grain size, water, and melt content.

Dunites

The upper mantle consists predominantly of olivine (≥60%) and pyroxene. Garnet, spinel, and (at shallow depth) plagioclase are minor phases. This suggests that deformation of the upper mantle is largely controlled by olivine. Extrapolation of laboratory data to geological deformation rates indicates that fine-grained (<50 μm) olivine aggregates (dunites) are predicted to deform dominantly by linear viscous creep with a stress exponent of $n \approx 1$ (**Figure 3**). The inverse dependence of creep rate on grain size was determined with a grain-size exponent of $m \approx 3$, indicating that creep is controlled by grain boundary diffusion. Diffusion creep is rate limited by the slowest diffusing ionic species along its fastest path. Recent results indicate that diffusion of silicon is rate-limiting diffusion creep of olivine at anhydrous and hydrous conditions (Hirth & Kohlstedt 2003, Mei & Kohlstedt 2000a).

With increasing differential stress (difference of maximum and minimum principal stress components), the dislocation creep of olivine aggregates becomes dominant at dry and wet experimental conditions. Several studies estimated a stress exponent of $n \approx 3$, irrespective of water content. By reanalyzing the data from Mei & Kohlstedt (2000b) and earlier studies, Hirth & Kohlstedt (2003) suggested a stress exponent of $n = 3.5 \pm 0.5$ for the dislocation creep of olivine rocks at hydrous and anhydrous conditions. Activation energies for dislocation creep found for both hydrous and anhydrous conditions (**Supplemental Table 1**) are in close agreement with $Q = 529$ kJ mol^{-1} estimated from silicon-diffusion experiments in olivine (Dohmen et al. 2002). This suggests that high-temperature dislocation creep of olivine is controlled by dislocation climb and is rate limited by diffusion of silicon (Kohlstedt 2007).

Simple-shear experiments performed in the dislocation creep regime reveal the importance of dynamic recrystallization and grain refinement in accommodating high strain in olivine aggregates. These experiments found that the evolution of a pronounced crystallographic texture reproduced deformation-induced lattice-preferred orientation observed in nature (Zhang & Karato 1995). Dynamic recrystallization and grain-size reduction were associated with a moderate weakening of up to 20%. Deformation textures continuously evolve up to shear strains of approximately five (Bystricky et al. 2000). This strain weakening adds to the uncertainties involved in extrapolating laboratory data from low-strain experiments to natural conditions.

For small grain size, relatively low temperatures, and elevated stresses, a grain-boundary-sliding regime is indicated at the transition between the diffusion and

dislocation creep fields for olivine deformed at anhydrous conditions (Hirth & Kohlstedt 2003). However, identification of grain boundary sliding as a dominant mechanism from mechanical data and microstructural observations remains difficult and is largely based on indirect evidence (Drury 2005).

Pressures in the upper mantle exceed those typically achieved in high-temperature deformation experiments by at least one order of magnitude. The effect of pressure on high-temperature creep depends on the rate-limiting diffusion and dislocation mechanisms. In the power-law equation, the pressure dependence is represented by an activation volume V, which is difficult to measure experimentally because of limitations related to pressure range and stress resolution in gas and solid medium apparatuses. Hence, estimates of the activation volume for creep are scarce.

Pyroxenites

Pyroxenes are major mineral constituents of lower-crustal granulites and upper-mantle peridotites, coexisting with the feldspar and olivine matrix phases, respectively. Constitutive equations now exist for calcium- and sodium-bearing clinopyroxenes such as diopside, omphacite, and jadeite (**Supplemental Table 1**). We focus on the constitutive behavior of diopside rocks for which data are available covering the diffusion and dislocation creep fields at hydrous and anhydrous conditions. Linear viscous creep dominated the mechanical behavior of diopside rocks at wet and dry conditions for stresses <200–300 MPa. The stress exponent $n \approx 1$ and grain-size exponent $m \approx 3$ indicate that creep at these conditions is dominantly controlled by grain boundary diffusion.

For fine-grained samples with a grain size of <40 μm, the transition from linear-viscous to power-law creep occurred at approximately 200–350 MPa differential stress. Investigators observed stress exponents between $n = 2.7 \pm 3$ and $n = 5.5$ in experiments on diopside samples performed at high stresses in the dislocation creep regime. A comparison of experiments performed on similar coarse-grained (>300 μm) natural samples reveals a substantial reduction of the stress exponent from $n = 4.7 \pm 0.2$ observed at dry conditions (Bystricky & Mackwell 2001) to $n = 2.7 \pm 0.3$ at wet conditions (Chen et al. 2006). In contrast to olivine rocks, activation energies for the high-temperature creep of pyroxenites are substantially lower at hydrous conditions. The effective viscosity of fine-grained samples deformed at anhydrous conditions is approximately one order of magnitude lower than that of coarse-grained samples from the same material (Bystricky & Mackwell 2001). The observed grain-size dependence in the dislocation creep regime may result from an increasing contribution of grain boundary sliding with decreasing grain size. The effect may be less pronounced at hydrous conditions, at which climb-controlled creep is more effective in diopside (Chen et al. 2006).

Anorthosites

Feldspar is the most abundant mineral phase in Earth's crust, contributing an average of approximately 60 wt% to igneous and metamorphic granitoids and gabbroic rocks.

The viscosity of the lower crust is thus largely determined by feldspar-dominated or at least feldspar-bearing rocks. In the past, studies of creep mechanisms operating in feldspar have largely focused on the analysis of experimentally produced deformation microstructures, which may be used to infer deformation mechanisms from field observations (Tullis 2002). Constitutive equations for synthetic anorthosites covering a broad range of thermodynamic conditions have been determined, but are still few (Rybacki & Dresen 2000, Rybacki et al. 2006).

At stresses below $\leq$200 MPa for wet samples and $\leq$100 MPa for dry specimens, diffusion-controlled creep is dominant at laboratory conditions, suggesting that the transition stress between dominant deformation mechanisms is affected by water content. Stress exponents of $n \approx 1.0$ and grain-size exponents of $m \approx 3$ indicate grain boundary diffusion controlled creep. Data also exist for diffusion creep of labradorite rocks deformed at hydrous conditions. Strength, stress exponent, and activation energy are similar within experimental error, suggesting that the viscosity of plagioclase rocks is not significantly affected by chemical composition (Dimanov et al. 2000). Experiments performed on feldspar rocks to large strain in torsion in the diffusion creep regime reveal an evolution of the microstructure, including creep damage and formation of a pronounced shape- and lattice-preferred orientation (Gomez-Barreiro et al. 2007). This texture evolution is possibly related to dislocation activity associated with grain boundary sliding, but this remains to be explored further.

Feldspar rocks deformed in the dislocation creep regime yield stress exponents of $n = 3$ irrespective of water content. As found in the diffusion creep regime, activation energies estimated under hydrous conditions are significantly lower than those obtained with dry samples (Rybacki & Dresen 2000). Deformation microstructures indicate dislocation glide, grain boundary migration, and recrystallization, but dislocation climb becomes important only at the highest experimental temperatures.

Quartzites

Numerous studies over the past 40 years have investigated the mechanical behavior of quartzites. However, high-resolution mechanical data from experiments performed in a gas apparatus under well-defined thermodynamic conditions are only now becoming available. Paterson (1989) pointed out the difficulty of equilibrating water-related point defect concentration with the environment at laboratory timescales. Consequently, recent studies of the deformation behavior of quartzites have focused on fully synthetic materials prepared with a sol-gel technique and the fabrication of very fine-grained rocks (<25 μm) from natural quartz powders hot pressed in the presence of water (Luan & Paterson 1992; Rutter & Brodie 2004a,b) (**Supplemental Table 1**).

Currently a single study is available that provides data for a diffusion creep flow law at hydrous conditions, determining a stress exponent of $n = 1 \pm 0.1$ and an activation energy of 220 ± 55 kJ mol^{-1} (Rutter & Brodie 2004a). Interestingly, a grain-size exponent $m = 2.0 \pm 0.8$ was estimated, indicating that the creep rate is controlled by volume diffusion (Nabbaro-Herring creep). When extrapolated to geological

conditions, the suggested flow law predicts viscosities that are substantially higher than those for quartz dislocation creep. Diffusion creep would only dominate at temperatures greater than 520°C, which appears to be at odds with geological evidence for linear viscous creep of fine-grained quartz mylonites observed at greenschist facies conditions (Behrmann 1985).

In the dislocation creep regime, Luan & Paterson (1992) determined stress exponents of $n = 2.3 \pm 0.3$ to 4.0 ± 0.8 depending on the starting material, and the corresponding activation energies are $Q = 148 \pm 46$ kJ mol^{-1} and $Q = 152 \pm 71$ kJ mol^{-1}. For specimens yielding a lower stress exponent, the authors inferred that grain boundary sliding substantially contributed to plastic flow. The activation energies and values found by Hirth et al. (2001) are also significantly lower than those estimated by Rutter & Brodie (2004b) (**Supplemental Table 1**). When extrapolated to geological conditions, recent quartzite flow laws, including solid medium data from Gleason & Tullis (1995), are bracketed by those of Rutter & Brodie (2004b) and Hirth et al. (2001), which all rapidly converge for stresses less than 50 MPa and temperatures of 450°C–500°C prevailing in the middle to lower crust.

Deformation Mechanisms Maps and Flow Laws

The mechanical behavior of dunites, pyroxenites, anorthosites, and quartzites for a range of conditions is depicted in the deformation mechanism maps in **Figure 3**. These maps can be presented in stress–grain size space and display laboratory data extrapolated to strain rates of 10^{-12} s^{-1}. The pyroxenite map is based on data from Dimanov & Dresen (2005), which gives somewhat higher viscosities at geological conditions compared with other studies (**Supplemental Table 1**). The choice is motivated by the observation that pyroxenes often form relatively strong porphyroclasts in feldspar- and olivine-dominated mylonites. The laboratory data presented in **Supplemental Table 1** and **Figures 1** and **3** deserve some additional comments.

First, silicate rocks deformed under hydrous conditions are significantly weaker than at anhydrous conditions. When the data are extrapolated to geological strain rates, the difference in strength and viscosity between wet and dry rocks may be as high as four orders of magnitude, depending on the temperature and deformation mechanism. The effect is commonly observed when only trace amounts of H_2O (for feldspar, approximately 0.02–0.5 wt% H_2O) are present in nominally anhydrous silicates as structurally bound point defects (structural hydroxyl) or dispersed fluid inclusions in grains or grain boundaries. Hydrolytic weakening was first detected for quartz by Griggs & Blacic (1965). Since then, investigators have suggested that the hydrolysis of Si-O-Si bonds and/or water-related changes of the point defect concentration in silicates may cause the observed weakening (Kohlstedt 2007). However, for most silicates except possibly for olivine, the understanding of the water-weakening mechanism is still limited.

We primarily present strength profiles and deformation mechanism maps for extrapolated data from rocks deformed under hydrous conditions. Several arguments suggest that anhydrous conditions on the level of water trace contents are likely the

exception in tectonically active areas. For example, deep-seated shear zones are frequently found to channel fluids, suggesting that hydrous conditions apply. Existing field estimates for the onset temperature of crystal plastic deformation (Pryer 1993, Voll 1976) are in agreement with extrapolated experimental data for quartzites and anorthosites deformed under hydrous conditions, but not with data from dry rocks. Whereas structurally bound defect concentrations of natural crustal and mantle rocks vary widely, hydroxyl concentrations up to 0.05 wt% H_2O are considered typical in feldspar (Johnson 2006). For crustal and mantle-derived pyroxenes, concentrations up to 0.05 and 0.1 wt% H_2O have been observed, respectively (Johnson 2006, Skogby 2006). These numbers are well in the range of water concentrations of rocks deformed experimentally under hydrous conditions.

Second, the deformation of lower-crustal and upper-mantle rocks may involve varying amounts of partial melt. The presence of a melt phase affects the viscosity of rocks in several ways (Renner et al. 2000). As a fluid, melt potentially reduces the effective confining pressure. A partial melt acts as a fast diffusion pathway in the grain matrix and locally enhances grain boundary sliding. These effects are well investigated for dunites and depend on the melt topology, which in turn is controlled by melt chemistry and the (anisotropic) solid-melt interfacial energies. A few recent investigations exist on partially molten granitic rocks and anorthosites (Dimanov et al. 2000, Rutter et al. 2006). For dunites with melt content up to 25% (Kohlstedt 2007), viscosity reduction for rocks deforming in diffusion and dislocation creep is well captured by an empirical relation of the form $\dot{\varepsilon}(\phi)/\dot{\varepsilon}(0) = \exp(\alpha\phi)$, where ϕ is the melt content and α is a constant varying between approximately 25 and 45 (e.g., Hirth & Kohlstedt 2003). For a melt content of 20%, a strain-rate enhancement of approximately two orders of magnitude is observed for dunites. At melt fractions beyond approximately 30%, the mechanical behavior may change from a framework-supported solid matrix to a particle-containing suspension. However, the critical melt fraction at which the matrix viscosity drops by orders of magnitude may be lower if large fractions of the grain boundaries are wetted by melt films. For example, in anorthosites, Dimanov et al. (2000) found that minor melt fractions of $\leq$3% forming grain boundary films reduced the viscosity by approximately 10 times. Field evidence indicates that some shear zones in high-temperature crustal and mantle rocks contain at least traces of melt, which probably lead to a much reduced strength compared to that of melt-free rocks (**Figure 1**).

Finally, experimental studies of polyphase rocks are still few. Most studies focus on mechanical interaction between two phases with different end-member viscosities. It is mostly found that the strength of synthetic polyphase rocks is bound by the strength of the respective end members. One may model the variation of strength as a function of phase content using empirical or continuum models (Dimanov & Dresen 2005, Tullis et al. 1991). However, viscosity may also be reduced by chemical reactions between minerals that result in reaction products with a grain size much finer than the reactants (de Ronde et al. 2005). In addition, second phase minerals, pores, and chemical impurities stabilize a fine grain size and indirectly promote linear viscous creep and softening of the rock (Herwegh et al. 2003).

VIEW FROM OUTER SPACE

Time-dependent deformation following a natural loading event (such as a large earthquake, the emplacement of a volcanic dike, the filling or draining of a lake, and the advance or withdrawal of a glacier) reflects the response of the structures and materials of the crust and upper mantle to rapid stress changes. Precise measurements and modeling of surface deformation, which results from relaxation of static stress changes by such loading events, allow us to probe the rheology of rocks deep in Earth. These events provide the opportunity to conduct giant rock-mechanics experiments in a natural laboratory of lithospheric dimensions.

During the past decade, great advances have been made in efforts to observe and explain transient postloading deformation thanks to much improved geodetic measurements and advances in deformation modeling software and computational hardware. Advances in geodetic techniques, especially the increased precision and spatial and temporal coverage of Global Positioning System (GPS) measurements (Segall & Davis 1997) and of Interferometric Synthetic Aperture Radar (InSAR) range-change data (Bürgmann et al. 2000), have led to vast improvements in our ability to detect and monitor time-dependent surface motions that reveal transient deformation processes at depth. Here we focus on recent progress made in inferences on lower-crustal and upper-mantle viscous rheology from geodetic measurements of postloading deformation. We provide an integrated view of studies ranging from explorations of rapid transients following historic large earthquakes to isostatic rebound of formerly glaciated regions that has been ongoing through the Holocene. **Supplemental Table 2** summarizes viscosity estimates from a number of studies.

Postseismic Deformation

The great 1906 San Francisco earthquake on the northern San Andreas Fault initiated not only the modern age of earthquake science, but also the use of geodesy to infer rheology at depth. Geodetic observations of deformation associated with the event led to the recognition of elastic rebound and the earthquake cycle (Reid 1910). Continued triangulation measurements in the decades following the earthquake revealed that postseismic accelerated deformation plays an important role (Thatcher 1983). Despite their relatively poor precision, the post-1906 deformation measurements have proven to be of great value in recent modeling studies attempting to elucidate the constitutive properties of the lithosphere. Kenner & Segall (2003) conclude that 90 years of post-1906 deformation data are best explained by models that incorporate weak vertical shear zones in the crust beneath major faults, as well as relaxation of a deep lower-crustal or mantle layer with effective viscosities of $\geq 9.5 \times 10^{19}$ Pa s.

A fundamental challenge to the use of postseismic deformation studies for improved understanding of rock rheology lies in the multitude of relaxation processes that follow earthquakes. Vigorous debate persists about what processes are responsible for the transient deformation, where the deformation occurs, and what the appropriate model representations of the candidate processes are. Models of distributed viscous shear and localized aseismic slip at depth can be parameterized to produce the same pattern of postseismic surface deformation for a two-dimensional, infinitely

long, strike-slip earthquake rupture. However, the resolution of the distribution of deep relaxation is not as ambiguous when considering three-dimensional postseismic deformation in a well-distributed network surrounding strike-slip ruptures with finite length (Hearn 2003).

The wide range of model interpretations of the crustal deformation following the 1992 $M_w = 7.4$ Landers and 1999 $M_w = 7.1$ Hector Mine earthquakes in the Mojave Desert of California illustrates the challenges and promises of postseismic studies to elucidate information about rheology at depth from geodetic measurements. Among the studies of the postseismic deformation following these events, some inferred primarily deep aseismic afterslip (Owen et al. 2002, Savage & Svarc 1997), whereas others considered only viscoelastic relaxation in the lower crust (Deng et al. 1998), a combination of poroelastic rebound and crustal afterslip (Fialko 2004, Peltzer et al. 1996), or poroelastic rebound and viscoelastic relaxation in the lower crust (Masterlark & Wang 2002). Pollitz et al. (2000, 2001) and Freed & Bürgmann (2004) found that the distribution of vertical and horizontal surface motions requires that the initial relaxation of the elastic earthquake stress primarily occurred in the upper mantle. Furthermore, Freed et al. (2007) identified deformation transients in continuous GPS time series at distances greater than 200 km from the Mojave earthquakes as strong evidence for a dominant contribution of broadly distributed mantle relaxation below a depth of 40 km. Poroelastic rebound and other crustal processes contribute to the near-field motions following the earthquakes; however, much of the time-dependent deformation following both Mojave Desert earthquakes results from flow in the mantle, below a stronger (i.e., relatively mafic, cold, and/or dry lithology) lower crust and ~10-km-thin lithospheric mantle lid. Owing to data limitations and inherent tradeoffs between contributions from various relaxation processes to the surface displacement field, it continues to be difficult to ascertain if lower-crustal deformation under the Mojave Desert faults is by distributed flow of a high-viscosity crust, by more localized ductile shear, or by frictional afterslip.

The rapid decay of the post-Landers and post–Hector Mine deformation transients is not consistent with the temporal evolution of deformation predicted by simple, linear flow models. Pollitz et al. (2001) suggested a time-dependent rheology in the upper mantle as a possible source of much reduced initial viscosities inferred for data obtained during the first year after the Hector Mine earthquake compared to values found from 1 to 3 years of deformation after Landers (Pollitz et al. 2000). The finding that inferred linear viscosities increase with time led Freed & Bürgmann (2004) to explore if elastic stress perturbations associated with the Mojave earthquakes are dissipated dominantly by power-law creep. They were able to fit the spatial and temporal patterns in the GPS data following both earthquakes with a model that relied on a mantle with experimentally determined flow-law parameters of wet olivine (Hirth & Kohlstedt 2003) and a geothermal gradient consistent with the upper range indicated by surface heat-flow measurements. Alternatively, Pollitz (2003) used the biviscous Burgers rheology (**Figure 2**) to model the rapid early deformation, which may reflect either power-law behavior or a weak, early transient rheology. Perfettini & Avouac (2007) matched the temporal evolution of 10 near-field, post-Landers GPS time series with a velocity-strengthening parameterization of a lower-crustal fault

zone, but did not take the contribution of deeper flow to this deformation explicitly into account.

The postseismic deformation following the 2002 $M_w = 7.9$ Denali fault earthquake in Alaska also suggests relaxation of the coseismic elastic stress field by a weak mantle below a relatively strong lower crust and uppermost mantle layer (Freed et al. 2006b), as well as a time-dependent rheology of the relaxing mantle (Freed et al. 2006a, Pollitz 2005). Freed et al. (2006b) found that best-fit effective mantle viscosities rapidly decrease from 10^{19} Pa s at the Moho at 50-km depth to 2–4 $\times$ 10^{18} Pa s at 100-km depth. A follow-up study (Freed et al. 2006a) suggests that rapidly decaying, far-field GPS time series reflect a stress-dependent mantle viscoelastic rheology (**Figure 4**). A power-law rheology, relying on experimentally derived parameters from Hirth & Kohlstedt (2003) and Rybacki & Dresen (2000), provides decay rates in agreement with observations. Lower-crustal relaxation contributes to the post-Denali deformation, but Freed et al. (2006b) could not uniquely determine if this relaxation came from a viscous ($>1 \times 10^{19}$ Pa s) layer or a localized shear zone. They favored localized shear owing to the observation of seismic velocity discontinuities across the fault down to a depth of ~60 km.

Studies of postseismic deformation following a number of other recent strike-slip earthquakes show that deep rheology differs depending on the local lithospheric structure and tectonics. Early postseismic transients following the $M_w = 7.4$ 1999 Izmit earthquake are more consistent with localized velocity-strengthening afterslip on the downdip extension of the coseismic rupture than with distributed flow (Hearn et al. 2002), but the continuing deformation transients in subsequent years suggest contributions from viscous flow in the lower crust and/or upper mantle (E.H. Hearn, S. Ergintav, R.E. Reilinger, and S. McClusky, manuscript in preparation). The $M_w = 7.6$ 1997 Manyi earthquake in Tibet, which ruptured the top ~20 km of the thickest section of continental crust on Earth (~70 km), was followed by transient deformation consistent with viscous relaxation of the lower crust with effective viscosities averaging 4 $\times$ 10^{18} Pa s. InSAR time series show that the effective viscosity increases over the 4-year observation, thus indicating stress-dependent viscous strength (Ryder et al. 2007). However, the InSAR range-change data can also be reproduced with a kinematic model of lower-crustal afterslip. Contributions from mantle flow below the ~70-km-thick Tibetan crust cannot be resolved by the InSAR data.

The discrimination of discrete afterslip versus distributed viscous flow is easier for earthquakes with a significant dip-slip component. For example, broad postseismic uplift following the 1959 $M_w = 7.3$ Hebken Lake normal-faulting earthquake in the northern Basin and Range province is consistent with a model of viscous relaxation of a low-viscosity (4×10^{18} Pa s) mantle below a 38-km-thick plate (Nishimura & Thatcher 2003). The data provide a lower-bound viscosity of 10^{20} Pa s for the lower crust. The observed uplift pattern rules out significant deep afterslip on or below the rupture, providing a more unique determination of the crustal source process than the strike-slip events discussed above. In contrast, the first 15 months of deformation following the $M_w = 7.8$ Chi-Chi thrust earthquake in Taiwan appear strongly dominated by afterslip, primarily on a décollement downdip of the coseismic rupture (Hsu et al. 2007).

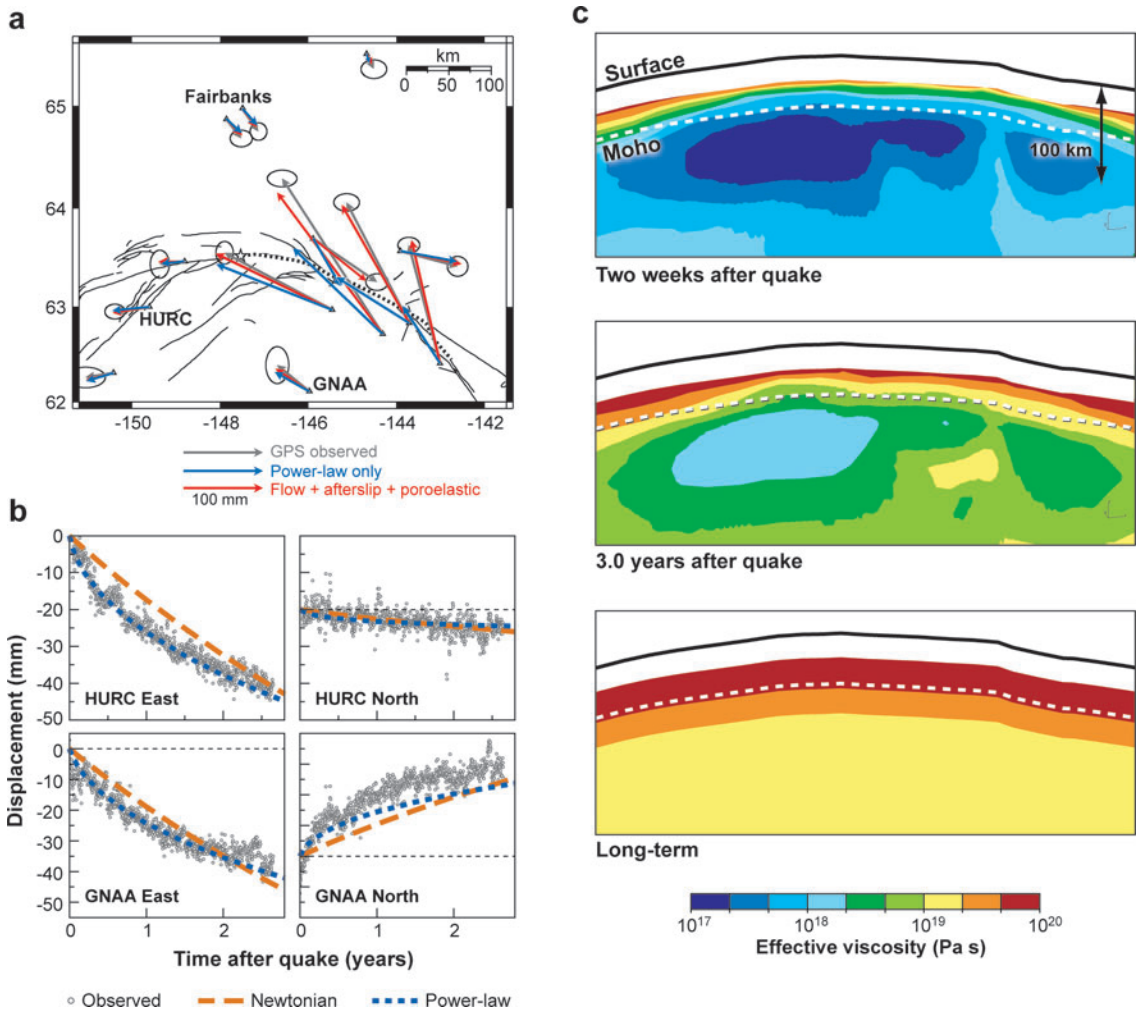

Figure 4

(*a*) Observed and modeled cumulative surface displacements during 3 years following the 2002 Denali earthquake. The epicenter of the earthquake is shown by a star and the dotted line indicates the surface rupture. The modeled displacements are based on a power-law model with an exponent of $n = 3.5$ in both the crust and upper mantle, which produced an optimal fit to the GPS time series, two of which are shown in panel *b*. The comparison of observed GPS position time series and displacements calculated by best-fit Newtonian ($n = 1$) and power-law models ($n = 3.5$) for two far-field stations shows that the rapid temporal decay cannot be matched by linear relaxation models. Annual, semiannual, and secular components have been removed from the observed time series. Power-law flow in the lower crust and upper mantle is sufficient to explain far-field displacements, whereas the addition of shallow afterslip and poroelastic rebound is required to explain near-field displacements. (*c*) Calculated effective viscosity from the power-law relaxation model along a cross section through the Denali fault as a function of time with respect to the Denali earthquake (modified from Freed et al. 2006a).

The duration and spatial extent of postseismic deformation scale with the size of the earthquake source. Thus, great subduction earthquakes produce the most enduring and far-reaching deformation transients from viscous relaxation in the upper mantle. Recently collected GPS data indicate that even four decades after the great $M_w = 9.3$ 1964 Alaska and $M_w = 9.5$ 1960 Chile megathrust ruptures, deformation rates are strongly perturbed landward of the rupture zones (Khazaradze & Klotz 2003, Zweck et al. 2002). Wang's (2007) review of viscous strength estimates for the upper mantle in the hanging wall of these and other subduction thrust earthquakes gives averages around 10^{19} Pa s. The 2004 $M_w = 9.2$ Sumatra-Andaman earthquake is the first $M > 9$ event to occur in the age of space geodesy, and monitoring of the postseismic deformation is beginning to reveal important information on mantle rheology in the region (Pollitz et al. 2006). Observed GPS time series from regional sites (mostly in Thailand and Indonesia), beginning in December 2004, compare well with models assuming a biviscous (Burgers body) mantle rheology. This model infers a transient viscosity of 5×10^{17} Pa s and a steady-state viscosity of 1×10^{19} Pa s, which dominate the early and late phase of the relaxation process in the backarc region of the Sumatra-Andaman events, respectively. As is the case with continental earthquakes, it is important to diagnose and separate substantial contributions to the measured surface motions from other processes, such as afterslip at seismogenic and greater depths.

We can draw several conclusions from the aggregate of postseismic studies. First, the mantle asthenosphere underlying several backarc and former backarc regions is viscously weak below 40-to-60-km thick crustal and uppermost-mantle layers. Second, the upper mantle in these tectonically active regions is approximately an order of magnitude weaker than the lower crust in the areas in which viscosity estimates exist for both. Third, the temporal evolution of postseismic relaxation in the uppermost mantle suggests time- and possibly stress-dependent viscous strength. Finally, postseismic stress relief in the lower-crustal downdip of a rupture may occur on localized, weakened shear zones and/or by more distributed flow.

Nontectonic Loading Events

Large earthquakes represent sudden, well-constrained stress-change events in Earth, but they occur along active fault zones and probe what might be anomalous lithospheric structure and rheology at depth (i.e., the ice cream in the banana split). Nontectonic loading events by lakes and glaciers offer the advantage of often examining rheology away from active faults, and challenges related to the trade-off between transient deep afterslip versus distributed viscous relaxation should be absent. Here, we consider relatively recent loading events from filling and fluctuations of manmade reservoirs and retreats of glaciers during the past few centuries, as well as effects from long-term fluctuations of large inland lake levels and continental ice sheets accompanying Holocene climate change.

Historic and more ancient changes in lake levels result in significant elastic stress fields that produce viscous flow at depth. Kaufmann & Amelung (2000) relied on 1932–1950 leveling measurements that document subsidence of approximately 0.2 m

following the filling of the Lake Mead reservoir in the southern Basin and Range province. Modeling the observed deformation as the response of a three-layer system, they found an upper-mantle viscosity on the order of 10^{18} Pa s and a lower-crustal viscosity of 4×10^{19} Pa s or more. Isostatic rebound of late-Pleistocene shorelines of paleolakes in the eastern (Lake Bonneville) and western (Lake Lahontan) Basin and Range province provides further constraints on mantle rheology underlying this region. Bills et al. (1994, 2007) modeled the uplift pattern of dated paleoshorelines and found that both regions appear to be underlain by low-viscosity mantle ($<10^{18}$ Pa s) between approximately 40 and 160 km, with slightly higher values inferred below 160 km. The long wavelength of the lake loads and observed rebound pattern make a reliable determination of lower-crustal flow strength difficult (B.G. Bills, personal communication).

Deformation following the retreat of glaciers during the past few centuries represents another opportunity to determine the mechanical properties of the underlying crust and mantle. In Iceland, the volume loss of the Vatnajökull ice cap since ~1890 results in active rebound rates up to 25 mm year^{-1}. Pagli et al. (2007) used 1996–2004 GPS velocities to infer a viscosity of $4–10 \times 10^{18}$ Pa s under a 10-to-20-km-thick elastic lid. In the Glacier Bay region of southeastern Alaska, Larsen et al. (2005) studied uplift in response to glacial retreat since ~1770 AD. The GPS-measured active deformation, with uplift rates as fast as 35 mm year^{-1}, together with tide gauge and shoreline data suggest an asthenosphere viscosity of 3.7×10^{18} Pa s in the upper mantle below a 60–70-km-thick lithosphere, consistent with results from the previously discussed post–Denali fault earthquake studies (Freed et al. 2006b).

Studies of surface deformation from ice-age glacial unloading cycles are at the far end of the spectrum in terms of the magnitude and spatial extent of the loading source and the duration and depth extent of viscous relaxation processes. Even thousands of years past the retreat of the Late Pleistocene glacial ice sheets over Scandinavia and North America, surface deformation in these regions is dominated by rapid uplift (up to ~10 mm year^{-1}), consistent with flow in the mantle toward the rebounding regions. Owing to the large wavelength of the ice load, the pattern of glacial isostatic adjustment provides information primarily about the viscosity structure deeper in the upper mantle and with limited vertical resolution. Active uplift in these regions has been known for some time and provided the first direct evidence of viscous mantle deformation (Haskell 1935).

Information about both horizontal and vertical motions from GPS measurements further improves the model resolution of the viscosity structure of Earth (Milne et al. 2001, Sella et al. 2007). Relying on a dense, three-dimensional GPS velocity field across Fennoscandia, Milne et al. (2001) estimated upper-mantle viscosities of $5–10 \times 10^{20}$ Pa s below a 90–170-km-thick elastic lithosphere (**Figure 5**). New space-based measurements of temporal changes in the gravity field over North America, with data from the GRACE (Gravity Recovery and Climate Experiment) satellite mission, complement studies relying on Earth-bound geodetic and geologic data (Tamisiea et al. 2007). The rate of gravity change during 2002–2006 is best fit by an upper-mantle viscosity of 8×10^{20} Pa s, underlying a 120-km-thick elastic lithosphere, consistent with earlier estimates. Recent studies begin to focus on the importance of lateral

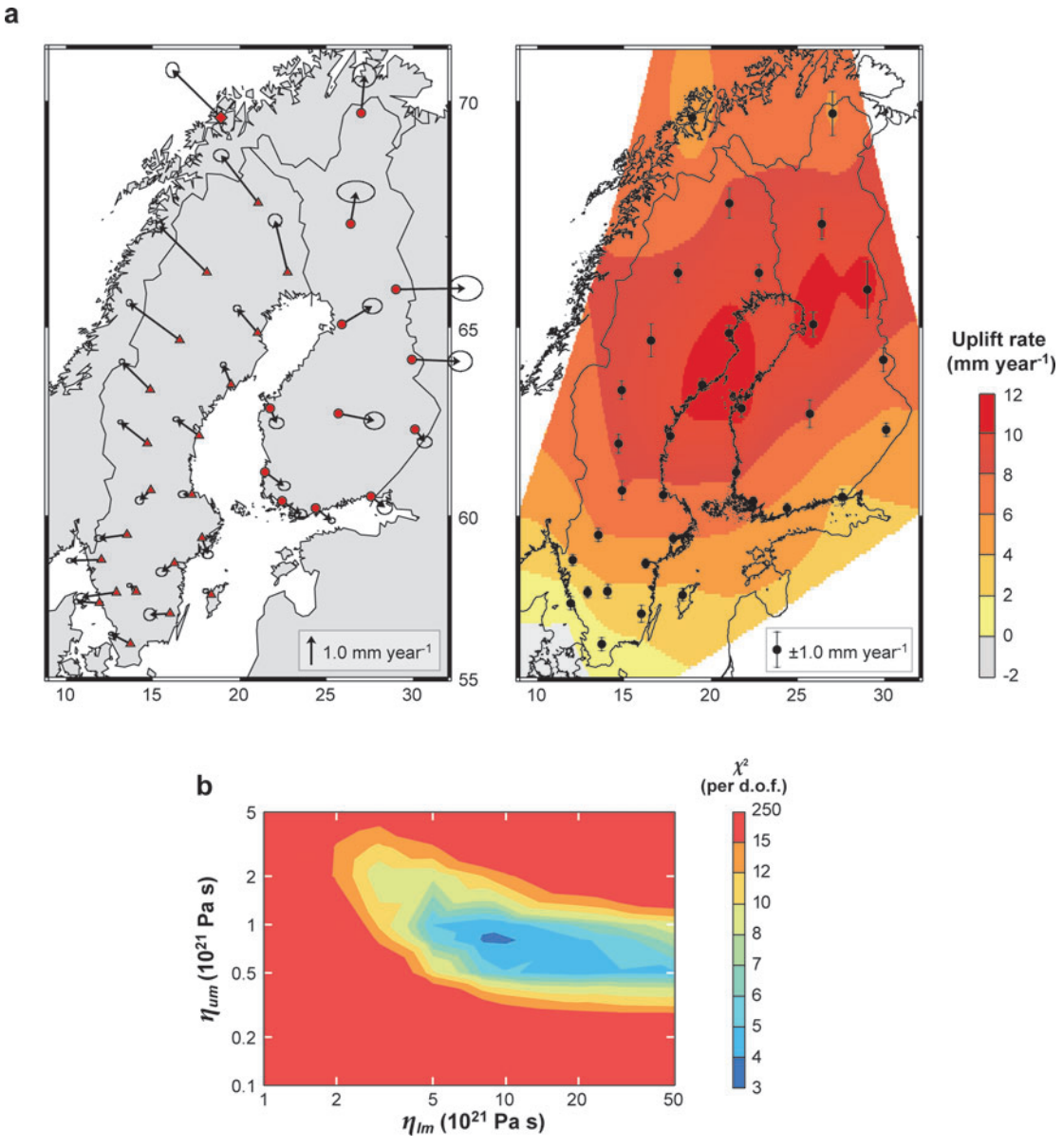

Figure 5

(*a*) Maps of present-day horizontal velocities and uplift rates in Fennoscandia. The vertical rate contours are constructed by fitting a polynomial function to rates obtained by GPS measurements. (*b*) The χ^2 misfit per degree of freedom between the three-dimensional GPS velocities and numerical glacial isostatic adjustment predictions. Misfit is shown as a function of η upper-mantle (η_{um}, above 670 km) and lower-mantle (η_{lm}) viscosities. The lithospheric thickness of Earth models was fixed to 120 km. Figure modified from Milne et al. 2001.

variations of lithosphere thickness and mantle structure in areas undergoing glacial isostatic adjustment, which one should account for when interpreting the increasingly detailed deformation measurements (Paulson et al. 2005, Wu 2005). Integration of paleo–sea level time series with the geodetically measured surface velocity field also allows for exploration of mantle power-law parameters (Wu 2002). Although there are important trade-offs between model parameters in glacial rebound studies, estimates of mantle viscosities underlying ~100-km-thick cratonic lithosphere within continental shield interiors lie in the range of $5–10 \times 10^{20}$ Pa s.

Holocene uplift patterns from glacial rebound over tectonically active regions, such as the northern Cascadia subduction zone and Iceland, suggest significantly lower effective mantle viscosities under thinner lithospheric lids than those found for cratonic shield regions. Modeling of shoreline tilts of proglacial lakes and rapid sea-level fall in southwestern British Columbia and Puget Sound following the retreat of the Cordilleran ice sheet suggests upper-mantle viscosities of $5–50 \times 10^{18}$ Pa s (James et al. 2000). This is in the range of estimates from models of Cascadia subduction-related deformation (Wang 2007) and various postseismic and recent lake-unloading studies in western North America (**Supplemental Table 2**). Holocene rebound of Iceland, located above a rising plume along the mid-Atlantic ridge, apparently completed in only ~1000 years in coastal areas and suggests a viscosity of less than 10^{19} Pa s (Sigmundsson 1991), again in the range of estimates from the more recent deformation events described above.

VIEW FROM THE FIELD

Current conceptual models of faults below the brittle regime are largely based on a synthesis of geological field studies, geophysical observations, and theoretical reasoning. Geophysical imaging provides some constraints on the deep architecture of fault zones. Geologic field studies reveal crucial information about the geometry of shear zones, processes governing shear zone nucleation and structural evolution, and the dominant physical mechanisms operating over a broad range of thermodynamic conditions and timescales. Field observations also reveal vertical gradients in rheology related to changes in material, fluid content, temperature, and pressure. Comparing shear zone microstructures with their experimental counterparts investigated in the laboratory helps identify deformation mechanisms that operate in Earth and determine large-scale fault dynamics. We focus on field studies of deep fault zones rather than of deformation below mostly undeformed crustal blocks.

Depth Extent of Fault Zones: Geophysical Imaging

The depth extent of large faults below the seismogenic zone and into the lower crust and upper mantle remains contentious. Deep sections of currently active faults are notoriously difficult to image using geophysical methods such as seismic or magnetotelluric measurements, and spatial resolution of available imaging techniques is severely limited at greater depths. Some geophysical studies of major strike-slip faults, such as the San Andreas Fault system and the Dead Sea transform, provide

Seismic anisotropy: anisotropy of shear wave velocities resulting from preferred crystallographic orientations and thus strain in rocks at depth

evidence of shear zones cutting through the entire crust (Henstock et al. 1997, Parsons & Hart 1999, Weber et al. 2004, Zhu 2000). In contrast, Wilson et al. (2004) argued that smoothly varying Moho depths and pervasive anisotropy below a 15-km depth under the Marlborough strike-slip fault zone show that lower-crustal deformation in New Zealand is broadly distributed.

The reach of well-defined fault zones into the mantle lithosphere is even less well resolved. Wittlinger et al. (1998) used tomographic imaging to argue for a ~40-km-wide mantle shear zone below the Altyn Tagh Fault in Tibet down to a >150-km depth, a zone that is also found to have increased and reoriented seismic anisotropy. However, significant seismic anisotropy is also found below seismic stations located in the interior of tectonic blocks in Tibet, away from the major faults, suggesting that mantle shear is distributed and not restricted to block-bounding fault zones (e.g., Sol et al. 2007). Based on the >300-km width of a zone displaying strong seismic anisotropy below the Alpine fault in New Zealand, Molnar et al. (1999) argue that mantle lithosphere beneath continental fault zones deforms by homogeneous shearing. In addition to providing information on the distribution of strain, the existence of a preferred lattice orientation in the upper ~200 km of the mantle also suggests that deformation to that depth likely occurs primarily by dislocation creep (Karato et al. 2008).

Micro- and Macrostructures of Exhumed Fault Zones

The application of laboratory-derived flow laws to processes occurring in Earth at much slower strain rates and lower stresses and/or temperatures relies in part on comparisons of microstructures observed in experimentally deformed samples with those in naturally deformed rocks. Microstructural studies of naturally deformed rocks allow the identification of dislocation creep and recrystallization mechanisms accommodating crystal plastic deformation (Tullis 2002). Criteria commonly considered diagnostic for grains-size-sensitive flow include a small grain size, equiaxial grains, homogeneously dispersed mineral phases, low dislocation densities, and a randomized weak or absent lattice-preferred orientation in high-strain rocks. However, recent experimental studies on feldspar aggregates clearly show that dislocation activity, recrystallization, and preferred orientation can develop in materials deforming to large strain under grain-size-sensitive flow (Dimanov et al. 2007, Gomez-Barreiro et al. 2007). This complicates a microstructure-based identification of the dominant deformation mechanism and inferences on the prevailing rheological behavior within shear zones.

A recurring observation from microstructural investigations is a significant reduction of grain size toward high shear strains (>1–10) resulting in intercalated fine-grained (<100-μm) ultramylonite layers. Processes leading to significant grain-size reduction of the host rock at the tip of propagating shear zones include dynamic recrystallization, cataclasis, and mineral reactions that produce fine-grained and weaker reaction products. In polycrystalline materials, mineral phases are relatively homogeneously dispersed or form grain-scale layers related to the destruction of porphyroclasts. Coexistence of high shear strain and small grain size in ultramylonites is often

rationalized with grain-size-sensitive creep controlled by grain boundary diffusion or dislocation activity. Ultramylonite layers seem to represent a final stage in shear zone evolution in which further localization is suppressed within the bands (Kenkmann & Dresen 2002).

Crustal Roots of Active Faults

Spectacular examples of active continental transforms with exposed mid- to lower-crustal roots are the Liquine-Ofqui Fault in southern Chile and the Alpine fault in New Zealand. Along both faults, ductile deformation structures from the lower crust were rapidly exhumed during episodes of transpression. Strikingly, the exposed deeper parts of these active faults appear extremely localized with shear zone widths of less than 5 km. At the Liquine-Ofqui fault, mylonites deformed at temperatures of up to ~500°C, and possibly higher, were partly overprinted by seismically active faults with similar kinematics. Exhumation rates of up to 2–3 mm year^{-1} (Thomson 2002) attest to rapid transpression-induced uplift and erosion along the fault zone. Structural studies reveal heterogeneous deformation in shear zones up to 5 km wide with intercalated mylonite and ultramylonite layers (Cembrano et al. 2002).

Along the surface trace of the Alpine fault, recent [<3–5 mya (Little et al. 2002)] transpression-induced exhumation exposed a 1–2-km-wide amphibolite-facies shear zone. This narrow mylonite zone is considered the relict downward extension of the Alpine fault. Mylonite deformation probably occurred down to a depth of 20–30 km at temperatures up to 550°C and pressures up to approximately 800 MPa (Little et al. 2002). Norris & Cooper (2003) suggested that the current 27 mm year^{-1} strike-slip rate along the Alpine fault has been relatively constant since the mid-Pliocene and may be accommodated entirely by ductile creep within the narrow mylonite shear zone at depth. Shear strain in the exhumed mylonites increases by more than one order of magnitude toward the trace of the active fault from approximately 10 in the protomylonite to 180–300 in ultramylonite layers (Norris & Cooper 2003). Close to the active fault trace of the Alpine fault, mylonites are cut by brittle faults and pseudotachylytes, reflecting the rise of the shear zone through the brittle-ductile transition zone (Sibson et al. 1979). A highly localized downward extension of the Alpine fault seems to contradict the finding of a distributed lower-crustal deformation zone from seismic imaging and anisotropy data by Wilson et al. (2004) across the northward continuation of the Alpine fault zone.

Fossil Shear Zones from Lower Crust and Upper Mantle

The roots of major transcurrent faults with lengths ranging between several tens of kilometers to approximately 1000 km are widely exposed in orogenic belts and deeply eroded interiors of continental shield areas. Although these shear zones are now inactive, detailed structural mapping and microstructural studies reveal characteristic patterns in their structural evolution and illuminate the deformation of mylonite rocks in the lower crust and upper mantle at pressures of up to >1 GPa and temperatures up to 1000°C. The width of the shear zones appears to narrow with decreasing

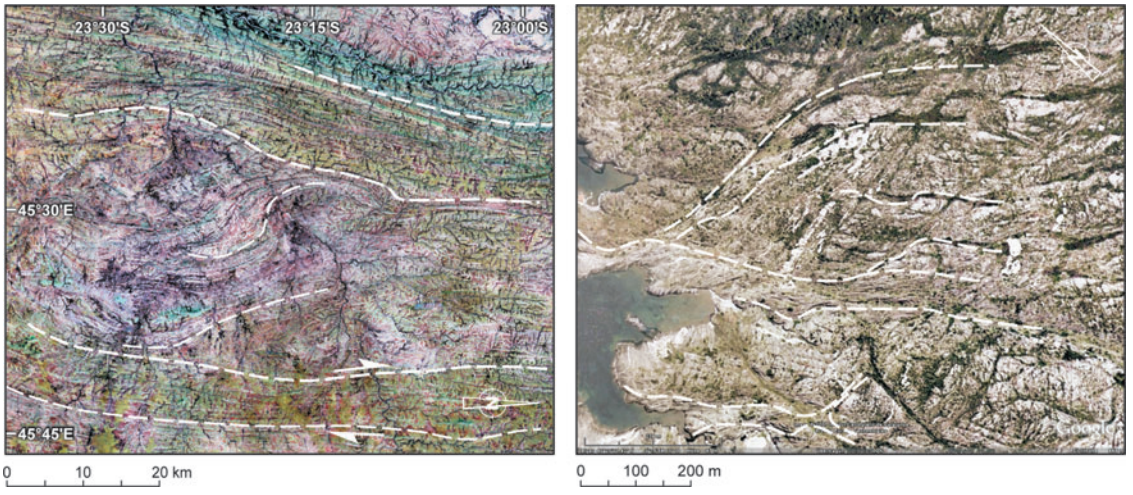

Figure 6

Satellite images of mylonite shear zones. (*Left panel*) Major shear belt in quartzo-feldspathic granulites (S. Madagascar, Martelat et al. 1999). Deformation occurred at higher amphibolite-to-granulite facies conditions at temperatures of approximately 700°C–800°C. (*Right panel*) A section of the Northern Cap de Creus shear belt in northeast Spain (Carreras 2001). The image shows an anastomosing network of shear zones cutting through metasedimentary rocks. Mylonites formed under greenschist facies conditions. Note the sigmoidal pattern of narrow mylonite layers surrounding lozenges of less deformed material. Imagery in right panel provided by Google Earth.

temperature and depth from granulite facies conditions up to the brittle-plastic transition zone in the middle crust. For deep crustal levels, mylonite belts with a width of up to >30 km have been reported that may narrow upward into 1–7-km-wide shear zones at amphibolite-greenschist facies conditions (Hanmer 1988, Vauchez & Tommasi 2003).

A characteristic feature of these large-scale shear zones is that they constitute anastomosing networks of densely intertwined mylonite layers with varying width, length, and total displacement, separating lozenges of less deformed material (**Figure 6**). Irrespective of the scale of observation, the internal structure of high-strain zones indicates the formation and growth of kinematically linked shear zone networks. These typically display slip transfer between cooperative shears and partitioning of strain between network structures, which are commonly observed from the regional scale down to the grain scale (Carreras 2001, Fusseis et al. 2006). Pronounced grain-size reduction in mylonite layers promotes strain localization and may substantially reduce the viscosity of shear zones in the lower crust compared to the host rock. Recent estimates suggest a viscosity reduction in shear zones up to a factor of approximately 100 (L. Mehl and G. Hirth, submitted manuscript).

High-strain shear zones are also frequently observed in exposed mantle peridotite massifs (e.g., Dijkstra et al. 2004, Vissers et al. 1995). In addition, there is evidence of shear localization in the subcontinental mantle from some mantle-derived

xenoliths (Gueguen & Nicolas 1980), and mylonites have also been found in dredged mid-ocean-ridge peridotites (Jaroslow et al. 1996). This suggests that shear zones could be relatively common in the uppermost mantle in which temperatures are lower and strength is commonly assumed to be highest. Pressure and temperature estimates from shear zones suggest these formed in situ or during the crustal emplacement of peridotite massifs at depth.

The observed mantle shear zone width varies from the several-kilometer scale down to ultramylonite layers that are just a few millimeters wide. Shear strain is often found to be accommodated in anastomosing networks of kinematically linked substructures consisting of mylonites and ultramylonite bands. Similar to their crustal counterparts, the localization and formation of mylonites correlate with significant grain-size reduction (Jin et al. 1998, Newman et al. 1999, Vissers et al. 1997). Some researchers have suggested that grain-size reduction promotes a transition from dislocation creep to linear-viscous and grain-size-sensitive flow, resulting in a large degree of softening of the upper mantle (e.g., Dijkstra et al. 2004, Jin et al. 1998), which may be enhanced by the presence of fluids and melts. For example, Dijkstra et al. (2002) argued for up to four orders of magnitude reduced viscosities in peridotite mylonites in the Othris peridotite massif in Greece that formed at temperatures of 800°C. These authors also suggest that the presence of feldspar clasts in a fine-grained matrix of dominantly olivine and pyroxene may indicate that mantle mylonites could be even weaker than coarse-grained feldspar-bearing crustal rocks. In a study of peridotite mylonites from oceanic mantle, Warren & Hirth (2006) suggested a weakening of more than four orders of magnitude at approximately 700°C compared to material outside of the shear zone. These observations all suggest that downward extensions of major plate-bounding faults in the upper mantle can contain localized shear zones with several orders of magnitude lower viscosities than undeformed mantle.

Titus et al. (2007) describe xenoliths brought up from ∼40-km depth (paleotemperatures of 970°C–1100°C) beneath the active San Andreas fault system that exhibit olivine lattice-preferred orientations, which they quantitatively compare to seismic anisotropy observations in the region. They support a model of a more broadly distributed (∼130-km) mantle shear zone below the San Andreas fault system. The common inference of broadly distributed mantle shear fabrics deep below active plate boundary zones from seismic anisotropy studies suggests that at increasing depth and temperatures, mantle deformation occurs by more coherent bulk flow. However, this does not preclude more localized shear zones embedded in the distributed shear fabric.

Grain-Size Data and Paleostress Estimates from Natural Shear Zones

Grain size appears to be a critical parameter reflecting the evolution of strength and deformation mechanisms in lithospheric shear zones. Recently, Evans (2005) suggested a state variable approach to account for evolving microstructure of rocks deformed to high strains to capture the transient evolution of strength with strain in appropriate constitutive equations. Ideally, it may be possible to identify a macroscopic measure that reflects varying rock strength and that could be included in a constitutive equation as an internal state variable. An obvious choice for such a state

variable is grain size because it reflects the strain-dependent breakdown process in the tip region of shear zones, it is readily measured from exposed rock samples, and an inverse relation between grain size and flow stress has been exploited extensively to establish paleopiezometers for different minerals (e.g., Twiss 1977, van der Wal et al. 1993). The grain size of mylonite and ultramylonite rocks from exposed lithospheric shear zones ranges from 5 μm up to ∼300 μm. Larger grain sizes in high-strain rocks are rarely observed, except for porphyroclasts that may have diameters up to several millimeters.

We compare dislocation flow laws for quartz, feldspar, pyroxenes, and olivine deformed experimentally at hydrous conditions with a comprehensive compilation of grain-size-derived stress estimates from shear zones from lower-crustal and upper-mantle exposures (**Figure 7**). These paleostress data are based on estimates provided in the literature or by conversion of the reported recrystallized grain-size data using the piezometric relation for feldspar from Twiss (1977). For upper-mantle shear zones, stress estimates are from the respective studies and are mostly based on the olivine piezometer suggested by van der Wal et al. (1993) or result from a comparison with extrapolated laboratory data. We find that the stress estimates from grain-size data broadly track the strength expected from feldspar- and olivine-dominated lithologies in the lower crust and upper mantle, respectively. Given the possibility that at decreasing grain size, diffusion creep becomes a more important deformation mechanism, some caution is indicated in the use of such stress estimates.

RECONCILING LABORATORY, GEODETIC, AND FIELD ESTIMATES OF RHEOLOGY

In the traditional jelly sandwich model of lithospheric rheology, a weak (ductile) lower crust overlies a strong upper mantle. Although such a model has prevailed over the past 20 years, several geodetic studies (summarized in **Supplemental Table 2**) suggest that the upper mantle (or the asthenospheric mantle below a very thin mantle lid) is actually weaker than the lower crust in many tectonically active regions. High temperatures and fluids can weaken the mantle in wide backarc regions or above rising mantle plumes. The range of lower-crustal viscosities obtained in post-loading geodetic studies (1 to $>10 \times 10^{19}$ Pa s) may be reconciled with feldspar- and pyroxene-dominated rocks deforming at hydrous conditions. Extrapolated laboratory findings indicate that dry and melt-free rocks have viscosities greater than 10^{20} Pa s at strain rates of approximately 10^{-12} s^{-1}, except at the highest temperatures, >900°C. Trace contents of H_2O on the order of 0.05–0.1 wt% are sufficient to reduce the viscosity of lower-crustal rocks but are insufficient to generate substantial amounts of partial melt in gabbroic rocks. Much lower viscosities ($1–10 \times 10^{16}$ Pa s)—which have been suggested in models of very weak lower-crustal channels comprising hydrolytically weakened, quartz-rich, and even partially melted materials—have not been probed in geodetic investigations. Lacking strong and thick lithospheric mantle roots, lithospheric strength in these regions may indeed be dominated by the crust as envisioned in the crème brûlée model. Mature plate boundary fault zones weaken as they evolve at all depth levels, supporting the view of lateral strength variation

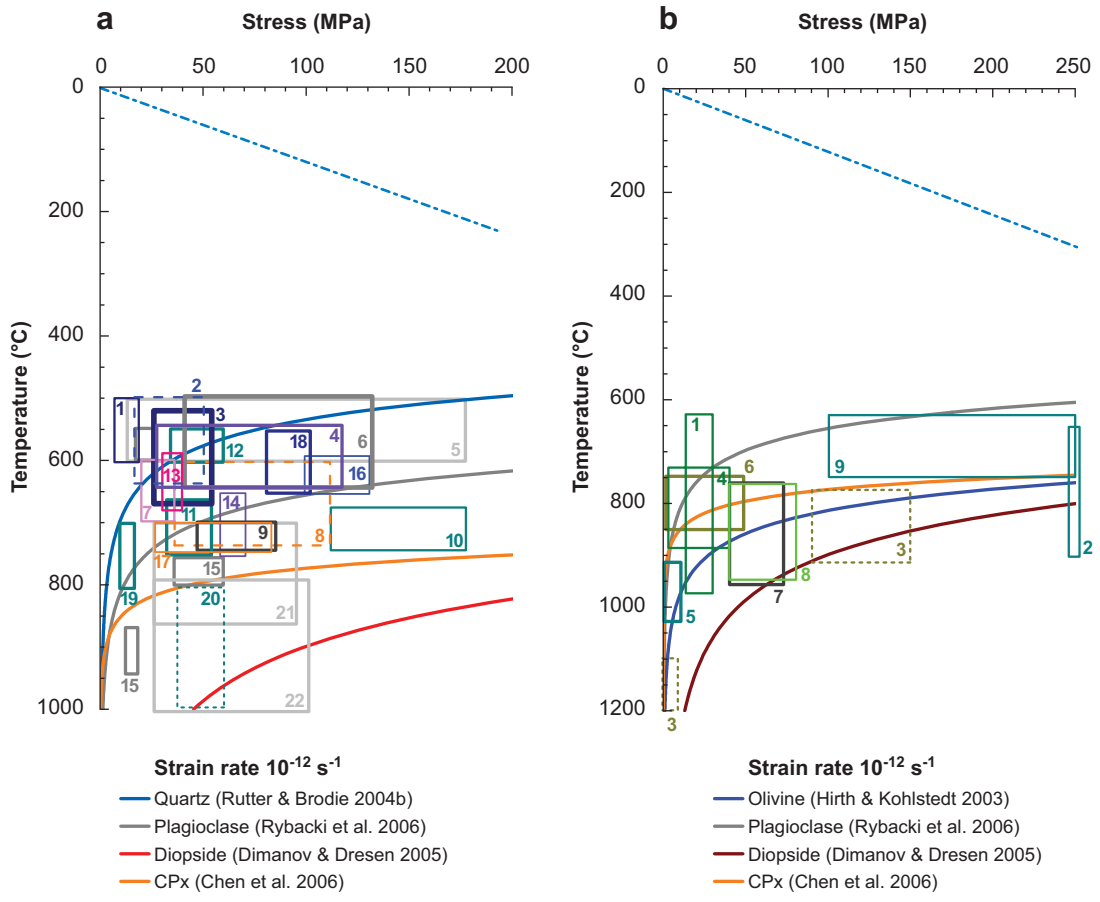

Figure 7

Paleostress estimates from mylonite shear zones transecting lower crust (*a*) and upper mantle (*b*). Each box represents stress-temperature estimates for a particular shear zone. A list with all numbered references is provided in the **Supplemental Appendix**. Stress estimates are mostly based on the inverse relation between recrystallized grain size and flow stress (Twiss 1977, van der Wal et al. 1993). Graphs indicate extrapolated laboratory data for the dislocation creep of rocks at hydrous conditions. The field data from lower-crustal shear zones are bracketed by the flow strength of quartzite and pyroxenite. Paleostress estimates from upper-mantle shear zones are bracketed by the flow strength of anorthosite and pyroxenite. The field estimates cluster between approximately 10 and 50 MPa in lower-crustal and upper-mantle shear zones. However, paleostresses could be severely overestimated if deformation in shear zones is dominated by diffusion-controlled creep.

envisioned by the banana split model. For example, the fine-grained matrix in mylonite shear zones in the lower crust and upper mantle favors grain-size-sensitive and possibly diffusion-controlled creep as the dominant deformation mechanisms (**Figure 3**). This suggests that in major shear zones, low viscosities could prevail to relatively low temperatures of ~500°C in the crust and ~700°C in the upper mantle.

Estimates of upper-mantle bulk rheology from geodetic and lab results appear to be quite consistent. Variations in mantle temperature, melt, and water content can account for the two-to-three order of magnitude difference we see in geodetic inferences of upper-mantle flow strength between continental shield regions and active plate boundary zones (**Supplemental Table 2**). Hyndman et al. (2005) suggested that the western North American Cordillera, and active and former backarc regions in general, is a region of hot upper mantle and lacks the thick and strong lithospheric lids of continental interiors. This is consistent with seismic tomography results showing wide regions of low seismic velocity and inferred high temperature underlying much of western North America (Goes & van der Lee 2002). Dixon et al. (2004) argued that addition of water from the subducting Farallon slab to the overlying mantle, as evidenced by geochemical studies of mantle xenoliths, further weakens mantle rheology below the tectonically active region. Model studies of glacial isostatic adjustment in North America and Fennoscandia agree on much higher upper-mantle viscosities and greater elastic plate thicknesses. This likely results from the location of these rebound regions over continental shields with relatively cold and dry mantle under thick, Precambrian-age lithospheres. The inferred variable upper-mantle viscosity structure is consistent with the extrapolation of experimental flow laws for dunite, assuming water-saturated conditions under western North America and anhydrous conditions or low-water content under the shield regions (Kohlstedt 2007).

An additional cause of variable effective viscosity estimates in geodetic studies lies in the nonlinear stress-strain relationship of deformation by dislocation creep. The rapid decay of postseismic transients following several of the earthquakes considered above requires time-dependent and likely stress-dependent viscous flow strength in the upper mantle. Dislocation creep is also indicated by the preferred mineral lattice orientations inferred from seismic observations of mantle anisotropy in the upper ~200 km of the mantle in many regions of the world. If rocks deform following a power law, viscosity varies as a function of ambient stress and thus decreases with time following a load step (**Figure 4**). The recognition of time-dependent viscous strength suggests that effective viscosities inferred from different loading events or observational time periods can differ by more than an order of magnitude. This mainly affects results obtained from data spanning the earliest relaxation phase (approximately the first year), which will greatly underestimate longer-term viscous strength. However, deformation by diffusion creep becomes dominant at low stress and small grain sizes, and we cannot simply assume that viscous deformation at depth is generally by $n \approx 3$ power-law creep. In fact, changes in stress through the earthquake cycle may possibly allow for repeated transitions between dominant deformation mechanisms below a fault zone. Drastic temporal variations in stress and strain rate from coseismic loading of deeper fault sections across the brittle-ductile transition are expected to produce episodic changes in dominant deformation modes, which can also lead to substantial and permanent structural changes and reduced strength in deep fault zones (e.g., Ellis et al. 2006, Handy et al. 2007).

Geologic field studies suggest ubiquitous localization of deformation in highly strained and weakened shear zones at all scales. Although geodetic studies often remain ambiguous with regards to the degree of localization of postseismic transient

deformation in the lower crust, we suspect that in many cases deformation is indeed localized in strain-weakened zones. Just below the brittle domain, shear zones may behave as frictional, velocity-strengthening fault zones, whereas at greater depth shear may occur by flow in narrow, low-viscosity shear zones, possibly embedded in wider deformation zones. The response of the upper mantle to loading events over a range of spatial and temporal scales as well as the observation of broad coherent mantle anisotropy suggest distributed flow. However, the recognition of localized peridotite shear zones in geologic field studies indicates that the distributed bulk shear may in part be accommodated in a heterogeneous fashion by a network of narrower shear zones, especially in the colder and stronger uppermost mantle.

SUMMARY POINTS

1. Robust constitutive equations exist for major constituents of the lower crust and upper mantle that appear consistent with field and geophysical observations. Viscosity estimates based on extrapolated laboratory data for pyroxenites, dunites, anorthosites, and quartzites deformed at hydrous conditions likely span the full range of flow strengths of rocks with a more complex mineralogical composition.
2. Lithospheric strength and rheology strongly differ as a function of the makeup, tectonic evolution, and environment of a region. Thus, rheology strongly varies with depth and across continental lithosphere of varying age, composition, and temperature. Competing simple models of lithosphere rheology should be considered as end-member cases only.
3. In backarc and former backarc regions, the upper mantle is viscously weaker than the lower crust owing to high temperatures and possibly the addition of water. Mantle below old cratonic shields is an order of magnitude stronger than that found in tectonically active regions.
4. Mature fault zones are weak, and deformation along them is localized to varying degrees throughout the lithosphere. The strength of the crust below seismogenic fault zones is weakened through earthquake-cycle effects and other strain weakening processes. Strain weakening up to several orders of magnitude and localization are ubiquitous at all scales.
5. Deformation in the uppermost mantle can also localize into mylonitic shear zones, but is probably more broadly distributed in the upper-mantle asthenosphere, in which it probably occurs by dislocation creep with a stress-dependent power-law rheology.
6. Deformation mechanisms and rheology depend on thermodynamic conditions, material parameters, and mechanical state and can vary over short distance scales (inside versus outside of a shear zone) and timescales (earthquake-cycle).

FUTURE ISSUES

1. Despite direct evidence for localized shear in the lowermost crust and upper mantle, we still do not know conclusively if lower-crustal deformation below active faults is always highly localized, broadly distributed, or transitioning from one to the other with depth. Future postseismic studies should be focused on resolving mid- to lower-crustal processes, and geophysical imaging tools need to be sharpened to better illuminate the deep architecture of active fault zones.
2. Transients in mechanical response due to abrupt or slow changes in loading, structural state, high strain, and other parameters remain to be explored in detail and should be included in appropriate constitutive relations. Laboratory studies need to further quantify flow parameters for partially molten and polyphase rocks. In particular, changes in rheology and weakening caused by metamorphic reactions are neither well understood nor quantified.
3. Geodetic explorations of deep rheology from postseismic deformation need to consider deformation early and late in the earthquake cycle and couple physically realistic model parameterizations of distributed plastic flow and localized shear. More postloading studies of all types are needed to better explore the distribution of lithospheric rheology across the continents and plate boundary zones.
4. Field studies should aim to quantitatively evaluate the distribution of strain in space and time as fault zones evolved. Detailed documentation of structural parameters such as grain size and its variation with shear strain, phase content, and temperature is needed, both within and away from high-strain shear zones.

DISCLOSURE STATEMENT

The authors are not aware of any biases that might be perceived as affecting the objectivity of this review.

ACKNOWLEDGMENTS

G.D. benefited from many fruitful discussions with Alex Dimanov, Brian Evans, Jörg Renner, and Erik Rybacki, who also provided help with the figures. R.B. acknowledges discussions and feedback from Andy Freed, Liz Hearn, Fred Pollitz, Wayne Thatcher, and Kelin Wang. The Alexander von Humboldt Stiftung supported a visit by R.B. at GFZ during which this article originated.

LITERATURE CITED

Behrmann JH. 1985. Crystal plasticity and superplasticity in quartzite: a natural example. *Tectonophysics* 115:101–29

Bills BG, Adams KD, Wesnousky SG. 2007. Viscosity structure of the crust and upper mantle in western Nevada from isostatic rebound patterns of Lake Lahontan shorelines. *J. Geophys. Res.* 112:B06405

Bills BG, Currey DR, Marshall GA. 1994. Viscosity estimates for the crust and upper mantle from patterns of lacustrine shoreline deformation in the Eastern Great Basin. *J. Geophys. Res.* 99:22059–86

Blanpied ML, Lockner DA, Byerlee JD. 1995. Frictional slip of granite at hydrothermal conditions. *J. Geophys. Res.* 100:13045–65

Brace WF, Kohlstedt DL. 1980. Limits on lithospheric stress imposed by laboratory experiments. *J. Geophys. Res.* 84:6248–52

Brudy M, Zoback MD, Fuchs K, Rummel F, Baumgärtner J. 1997. Estimation of the complete stress tensor to 8 km depth in the KTB scientific drill holes: implications for crustal strength. *J. Geophys. Res.* 102:18453–76

Bürgmann R, Rosen PA, Fielding EJ. 2000. Synthetic aperture radar interferometry to measure Earth's surface topography and its deformation. *Annu. Rev. Earth Planet. Sci.* 28:169–209

Burov EB, Watts AB. 2006. The long-term strength of continental lithosphere: "jelly sandwich" or "crème brûlée"? *GSA Today* 12:4–10

Byerlee J. 1978. Friction of rocks. *Pure Appl. Geophys.* 116:615–26

Bystricky M, Kunze K, Burlini L, Burg JP. 2000. High shear strain of olivine aggregates: rheological and seismic consequences. *Science* 290:1564–67

Bystricky M, Mackwell S. 2001. Creep of dry clinopyroxenite aggregates. *J. Geophys. Res.* 106:13443–54

Carreras J. 2001. Zooming on Northern Cap de Creus shear zones. *J. Struct. Geol.* 23:1457–86

Cembrano J, Lavenu A, Reynolds P, Arancibia G, Lopez G, Sanhueza A. 2002. Late Cenozoic transpressional ductile deformation north of the Nazca–South America–Antarctica triple junction. *Tectonophysics* 354:289–314

Chen S, Hiraga K, Kohlstedt DL. 2006. Water weakening of clinopyroxene in the dislocation creep regime. *J. Geophys. Res.* 111:B08203

Deng J, Gurnis M, Kanamori H, Hauksson E. 1998. Viscoelastic flow in the lower crust after the 1992 Landers, California, earthquake. *Science* 282:1689–92

de Ronde AA, Stunitz H, Tullis J, Heilbronner R. 2005. Reaction-induced weakening of plagioclase-olivine composites. *Tectonophysics* 409:85–106

Dijkstra AH, Drury MR, Vissers RLM, Newman J. 2002. On the role of melt-rock reaction in mantle shear zone formation in the Othris peridotite massif (Greece). *J. Struct. Geol.* 24:1431–50

Dijkstra AH, Drury MR, Vissers RLM, Newman J, Van Roermund HLM. 2004. Shear zones in the upper mantle: evidence from alpine- and ophiolite-type peridotite massifs. *Geol. Soc. Lond. Spec. Pub.* 224:11–24

Dimanov A, Dresen G. 2005. Rheology of synthetic anorthite-diopside aggregates: implications for ductile shear zones. *J. Geophys. Res.* 110:B07203

Dimanov A, Rybacki E, Wirth R, Dresen G. 2007. Creep and strain-dependent microstructures of synthetic anorthite-diopside aggregates. *J. Struct. Geol.* 29:1049–69

Dimanov A, Wirth R, Dresen G. 2000. The effect of melt distribution on the rheology of plagioclase rocks. *Tectonophysics* 328:307–27

Dixon JE, Dixon TH, Bell DR, Malservisi R. 2004. Lateral variation in upper mantle viscosity: role of water. *Earth Planet. Sci. Lett.* 222:451–67

Dohmen R, Chakraborty S, Becker H-W. 2002. Si and O diffusion in olivine and implications for characterizing plastic flow in the mantle. *Geophys. Res. Lett.* 29:2030

Drury MR. 2005. Dynamic recrystallization and strain softening of olivine aggregates in the laboratory and the lithosphere. *Geol. Soc. Lond. Spec. Pub.* 243:143–58

Ellis S, Beavan J, Eberhart-Phillips D, Stöckhert B. 2006. Simplified models of the Alpine Fault seismic cycle: stress transfer in the mid-crust. *Geophys. J. Int.* 166:386–402

Evans B. 2005. Creep constitutive laws for rocks with evolving structure. *Geol. Soc. Lond. Spec. Pub.* 245:329–46

Fialko Y. 2004. Evidence of fluid-filled upper crust from observations of postseismic deformation due to the 1992 M_w7.3 Landers earthquake. *J. Geophys. Res.* 109:B08401

Freed AM, Bürgmann R. 2004. Evidence of power-law flow in the Mojave desert mantle. *Nature* 430:548–51

Freed AM, Bürgmann R, Calais E, Freymueller JT. 2006a. Stress-dependent power-law flow in the upper mantle following the 2002 Denali, Alaska, earthquake. *Earth Planet. Sci. Lett.* 252:481–89

Freed AM, Bürgmann R, Calais E, Freymueller JT, Hreinsdóttir S. 2006b. Implications of deformation following the 2002 Denali, Alaska, earthquake for postseismic relaxation processes and lithospheric rheology. *J. Geophys. Res.* 111:B01401

Freed AM, Bürgmann R, Herring TA. 2007. Far-reaching transient motions after Mojave earthquakes require broad mantle flow beneath a strong crust. *Geophys. Res. Lett.* 34:L19302

Fusseis F, Handy MR, Schrank C. 2006. Networking of shear zones at the brittle-to-viscous transition (Cap de Creus, NE Spain). *J. Struct. Geol.* 28:1228–43

Gleason GC, Tullis J. 1995. A flow law for dislocation creep of quartz aggregates determined with the molten salt cell. *Tectonophysics* 247:1–23

Goes S, van der Lee S. 2002. Thermal structure of the North American uppermost mantle inferred from seismic tomography. *J. Geophys. Res.* 107:2050

Goetze C, Evans B. 1979. Stress and temperature in the bending lithosphere as constrained by experimental rock mechanics. *Geophys. J. R. Astron. Soc.* 59:463–78

Gomez-Barreiro J, Lonardelli I, Wenk HR, Dresen G, Rybacki E, et al. 2007. Orientation of anorthite deformed experimentally in Newtonian creep. *Earth Planet. Sci. Lett.* 264:188–207

Griggs DT, Blacic JD. 1965. Quartz: anomalous weakness of synthetic crystals. *Science* 147:292–95

Gueguen Y, Nicolas A. 1980. Deformation of mantle rocks. *Annu. Rev. Earth Planet. Sci.* 8:119–44

Handy MR, Hirth G, Bürgmann R. 2007. Continental fault structure and rheology from the frictional-to-viscous transition downward. In *Tectonic Faults: Agents of Change on a Dynamic Earth*, ed. MR Handy, G Hirth, N Hovius, pp. 139–81. Cambridge, MA: MIT

Hanmer S. 1988. Great Slave Lake shear zone, Canadian shield: reconstructed vertical profile of a crustal-scale fault zone. *Tectonophysics* 149:245–64

Haskell NA. 1935. The motion of a fluid under a surface load. *Physics* 6:265–69

Hearn EH. 2003. What can GPS data tell us about the dynamics of post-seismic deformation? *Geophys. J. Int.* 155:753–77

Hearn EH, Bürgmann R, Reilinger R. 2002. Dynamics of Izmit earthquake postseismic deformation and loading of the Duzce earthquake hypocenter. *Bull. Seism. Soc. Am.* 92:172–93

Henstock TJ, Levander A, Hole JA. 1997. Deformation in the lower crust of the San Andreas fault system in northern California. *Science* 278:650–53

Herwegh M, Xiao X, Evans B. 2003. The effect of dissolved magnesium on diffusion creep in calcite. *Earth Planet. Sci. Lett.* 212:457–70

Hetland EA, Hager BH. 2006. The effects of rheological layering on postseismic deformation. *Geophys. J. Int.* 166:277–92

Hirth G, Kohlstedt DL. 2003. Rheology of the upper mantle and the mantle wedge: a view from the experimentalists. In *Inside the Subduction Factory*, ed. J Eiler, pp. 83–105. *Geophys. Monogr.* 138. Washington, DC: Am. Geophys. Soc.

Hirth G, Teyssier C, Dunlap WJ. 2001. An evaluation of quartzite flow laws based on comparisons between experimentally and naturally deformed rocks. *Int. J. Earth Sci.* 90:77–87

Hsu Y-J, Segall P, Yu SB, Kuo L-C, Williams CA. 2007. Temporal and spatial variations of postseismic deformation following the 1999 Chi-Chi, Taiwan earthquake. *Geophys. J. Int.* 169:367–79

Hyndman RD, Currie CA, Mazzotti SP. 2005. Subduction zone backarcs, mobile belts, and orogenic heat. *GSA Today* 15:4–10

Jackson J. 2002. Strength of the continental lithosphere: time to abandon the jelly sandwich? *GSA Today* 12:4–9

James TS, Clague JJ, Wang K, Hutchinson I. 2000. Postglacial rebound at the northern Cascadia subduction zone. *Q. Sci. Rev.* 19:1527–41

Jaroslow GE, Hirth G, Dick HJB. 1996. Abyssal peridotite mylonites: implications for grain-size sensitive flow and strain localization in the oceanic lithosphere. *Tectonophysics* 256:17–37

Jin D, Karato S, Obata M. 1998. Mechanisms of shear localization in the continental lithosphere: inference from the deformation microstructures of peridotites from the Ivrea zone, northwestern Italy. *J. Struct. Geol.* 20:195–209

Johnson EA. 2006. Water in nominally anhydrous crustal minerals: speciation, concentration, and geologic significance. In *Water in Nominally Anhydrous Minerals*, ed. JR Smith, H Keppler, pp. 117–54. Chantilly, VA: Mineral. Soc. Am.

Karato S-I, Jung H, Katayama I, Skemer P. 2008. Geodynamic significance of seismic anisotropy of the upper mantle: new insights from laboratory studies. *Annu. Rev. Earth Planet. Sci.* 36: In press

Kaufmann G, Amelung F. 2000. Reservoir-induced deformation and continental rheology in the vicinity of Lake Mead, Nevada. *J. Geophys. Res.* 105:16341–58
Kenkmann T, Dresen G. 2002. Dislocation microstructures and phase distribution in a lower crustal shear zone: an example from the Ivrea-Zone, Italy. *Int. J. Earth Sci.* 91:445–58
Kenner SJ, Segall P. 2003. Lower crustal structure in northern California: implications from strain-rate variations following the 1906 San Francisco earthquake. *J. Geophys. Res.* 108:2011
Khazaradze G, Klotz J. 2003. Short- and long-term effects of GPS measured crustal deformation rates along the south central Andes. *J. Geophys. Res.* 108:2289
Kohlstedt DL. 2007. Constitutive equations, rheological behavior, and viscosity of rocks. In *Treatise on Geophysics*, ed. G Schubert, Vol. 2, *Miner. Phys.* Amsterdam: Elsevier. In press
Larsen CF, Motyka RJ, Freymueller JT, Echelmeyer KA, Ivins ER. 2005. Rapid viscoelastic uplift in southeast Alaska caused by post–Little Ice Age glacial retreat. *Earth Planet. Sci. Lett.* 237:548–60
Little TA, Holcombe RJ, Ilg BR. 2002. Kinematics of oblique collision and ramping inferred from microstructures and strain in middle crustal rocks, central Southern Alps, New Zealand. *J. Struct. Geol.* 24:219–39
Luan FC, Paterson MS. 1992. Preparation and deformation of synthetic aggregates of quartz. *J. Geophys. Res.* 97:301–20
Marone CJ. 1998. Laboratory-derived friction laws and their application to seismic faulting. *Annu. Rev. Earth Planet. Sci.* 26:643–96
Martelat JE, Schulmann K, Lardeaux JM, Nicollet C, Cardon H. 1999. Granulite microfabrics and deformation mechanisms in southern Madagascar. *J. Struct. Geol.* 21:671–87
Masterlark T, Wang HF. 2002. Transient stress coupling between the 1992 Landers and 1999 Hector Mine, California, earthquakes. *Bull. Seism. Soc. Am.* 92:1470–86
Mei S, Kohlstedt DL. 2000a. Influence of water on plastic deformation of olivine aggregates 1. Diffusion creep regime. *J. Geophys. Res.* 105:21457–69
Mei S, Kohlstedt DL. 2000b. Influence of water on plastic deformation of olivine aggregates 2. Dislocation creep regime. *J. Geophys. Res.* 105:21471–81
Milne GA, Davis JL, Mitrovica JX, Scherneck H-G, Johansson JM, et al. 2001. Space-geodetic constraints on glacial isostatic adjustment in Fennoscandia. *Science* 291:2381–85
Molnar P, Anderson HJ, Audoine E, Eberhart-Phillips D, Gledhill KR, et al. 1999. Continuous deformation versus faulting through the continental lithosphere of New Zealand. *Science* 286:516–19
Newman J, Lamb WM, Drury MR, Vissers RLM. 1999. Deformation processes in a peridotite shear zone: reaction softening by an H_2O-deficient, continuous net transfer reaction. *Tectonophysics* 303:193–222
Nishimura T, Thatcher W. 2003. Rheology of the lithosphere inferred from postseismic uplift following the 1959 Hebgen Lake earthquake. *J. Geophys. Res.* 108:2389
Norris RJ, Cooper AF. 2003. Very high strains recorded in mylonites along the Alpine Fault, New Zealand: implications for the deep structure of plate boundary faults. *J. Struct. Geol.* 25:2141–57

Owen S, Anderson G, Agnew DC, Johnson H, Hurst K, et al. 2002. Early Postseismic deformation from the 16 October 1999 M_w7.1 Hector Mine, California, earthquake as measured by survey-mode GPS. *Bull. Seism. Soc. Am.* 92:1423–32

Pagli C, Sigmundsson F, Lund B, Sturkell E, Geirsson H, et al. 2007. Glacio-istostatic deformation around the Vatnajökull ice cap, Iceland, induced by recent climate warming: GPS observations and finite element modeling. *J. Geophys. Res.* 112:B08405

Parsons T, Hart PE. 1999. Dipping San Andreas and Hayward faults revealed beneath San Francisco Bay, California. *Geology* 27:839–42

Paterson MS. 1989. The interaction of water with quartz and its influence in dislocation flow: an overview. In *Rheology of Solids and of the Earth*, ed. S Karato, M Toriumi, pp. 107–42. New York: Oxford Univ. Press

Paulson A, Zhong S, Wahr J. 2005. Modelling postglacial rebound with lateral viscosity variations. *Geophys. J. Int.* 163:357–71

Peltzer G, Rosen P, Rogez F, Hudnut K. 1996. Postseismic rebound in fault stepovers caused by pore fluid flow. *Science* 273:1202–4

Perfettini H, Avouac JP. 2007. Modeling afterslip and aftershocks following the 1992 Landers Earthquake. *J. Geophys. Res.* 112:B07409

Pollitz FF. 2003. Transient rheology of the uppermost mantle beneath the Mojave Desert, California. *Earth Planet. Sci. Lett.* 215:89–104

Pollitz FF. 2005. Transient rheology of the upper mantle beneath central Alaska inferred from the crustal velocity field following the 2002 Denali earthquake. *J. Geophys. Res.* 11:B08407

Pollitz FF, Bürgmann R, Banerjee P. 2006. Post-seismic relaxation following the great 2004 Sumatra-Andaman earthquake on a compressible self-gravitating Earth. *Geophys. J. Int.* 167:397–420

Pollitz FF, Peltzer G, Bürgmann R. 2000. Mobility of continental mantle: evidence from postseismic geodetic observations following the 1992 Landers earthquake. *J. Geophys. Res.* 105:8035–54

Pollitz FF, Wicks C, Thatcher W. 2001. Mantle flow beneath a continental strike-slip fault: postseismic deformation after the 1999 Hector Mine earthquake. *Science* 293:1814–18

Pryer LL. 1993. Microstructures in feldspars from a major crustal thrust zone: the Grenville Front, Ontario, Canada. *J. Struct. Geol.* 15:21–36

Reid HF. 1910. Permanent displacements of the ground, in the California earthquake of April 18, 1906. In *Report of the State Earthquake Investigation Commission*, pp. 16–28. Washington, D.C.: Carnegie Inst. Wash.

Reiner M. 1964. The Deborah number. *Phys. Today*: 62

Renner J, Evans B, Hirth G. 2000. On the rheologically critical melt fraction. *Earth Planet. Sci. Lett.* 181:585–94

Rutter EH, Brodie KH. 2004a. Experimental grain size-sensitive flow of hot-pressed Brazilian quartz aggregates. *J. Struct. Geol.* 26:2011–23

Rutter EH, Brodie KH. 2004b. Experimental intracrystalline plastic flow in hot-pressed synthetic quartzite prepared from Brazilian quartz crystals. *J. Struct. Geol.* 26:259–70

Rutter EH, Brodie KH, Irving DH. 2006. Flow of synthetic, wet, partially molten "granite" under undrained conditions: an experimental study. *J. Geophys. Res.* 111:B06407

Rybacki E, Dresen G. 2000. Dislocation and diffusion creep of synthetic anorthite aggregates. *J. Geophys. Res.* 105:26017–36

Rybacki E, Gottschalk M, Wirth R, Dresen G. 2006. Influence of water fugacity and activation volume on the flow properties of fine-grained anorthite aggregates. *J. Geophys. Res.* 111:B03203

Ryder I, Parsons BE, Wright TJ, Funning GJ. 2007. Post-seismic motion following the 1997 Manyi (Tibet) earthquake: InSAR observations and modeling. *Geophys. J. Int.* 169:1009–27

Savage JC, Svarc JL. 1997. Postseismic deformation associated with the 1992 M_w = 7.3 Landers earthquake, southern California. *J. Geophys. Res.* 102:7565–77

Segall P, Davis JL. 1997. GPS applications for geodynamics and earthquake studies. *Annu. Rev. Earth Planet. Sci.* 25:301–36

Sella GF, Stein S, Dixon TH, Craymer M, James TS, et al. 2007. Observation of glacial isostatic adjustment in stable North America with GPS. *Geophys. Res. Lett.* 34:L02306

Sibson RH, White SH, Atkinson BK. 1979. Fault rock distribution and structure within the Alpine Fault Zone: a preliminary account. *Bull. R. Soc. N.Z.* 18:55–65

Sigmundsson F. 1991. Post-glacial rebound and asthenosphere viscosity in Iceland. *Geophys. Res. Lett.* 18:1131–34

Skogby H. 2006. Water in natural mantle minerals I: pyroxenes. In *Water in Nominally Anhydrous Minerals*, ed. JR Smith, H Keppler, pp. 155–67. Chantilly, VA: Mineral. Soc. Am.

Sol S, Meltzer A, Bürgmann R, van der Hilst RD, King R, et al. 2007. Geodynamics of the southeastern Tibetan plateau from seismic anisotropy and geodesy. *Geology* 35:563–66

Tamisiea ME, Mitrovica JX, Davis JL. 2007. GRACE gravity data constrain ancient ice geometries and continental dynamics over Laurentia. *Science* 316:881–83

Thatcher W. 1983. Nonlinear strain buildup and the earthquake cycle on the San Andreas fault. *J. Geophys. Res.* 88:5893–902

Thomson SN. 2002. Late Cenozoic geomorphic and tectonic evolution of the Patagonian andes between 42°S and 46°S: an appraisal based on fission-track results from the transpressional intra-arc Liquine-Ofqui fault zone. *Geol. Soc. Am. Bull.* 114:1159–73

Titus SJ, Medaris LG, Wang HF, Tikoff B. 2007. Continuation of the San Andreas fault system into the upper mantle: evidence from spinel peridotite xenoliths in the Coyote Lake basalt, central California. *Tectonophysics* 429:1–20

Tse ST, Rice JR. 1986. Crustal earthquake instability in relation to the depth variation of frictional slip properties. *J. Geophys. Res.* 91:9452–72

Tullis J. 2002. Deformation of crustal materials. *Rev. Mineral.* 51:51–95

Tullis TE, Horowitz FG, Tullis J. 1991. Flow laws of polyphase aggregates from end-member flow laws. *J. Geophys. Res.* 96:8081–96

Twiss RJ. 1977. Theory and applicability of a recrystallized grain size paleopiezometer. *Pure Appl. Geophys.* 115:227–44

van der Wal D, Chopra P, Drury M, FitzGerald J. 1993. Relationships between dynamically recrystallized grain size and deformation conditions in experimentally deformed olivine rocks. *Geophys. Res. Lett.* 20:1479–82

Vauchez A, Tommasi A. 2003. Wrench faults down to the asthenosphere: geological and geophysical evidence and thermomechanical effects. *Geol. Soc. Lond. Spec. Pub.* 210:15–34

Vissers RLM, Drury MR, Newman J, Fliervoet TF. 1997. Mylonitic deformation in upper mantle peridotites of the North Pyrenean Zone (France): implications for strength and strain localization in the lithosphere. *Tectonophysics* 279:303–25

Vissers RLM, Drury MR, Strating EHH, Spiers CJ, van der Wal D. 1995. Mantle shear zones and their effect on lithosphere strength during continental breakup. *Tectonophysics* 249:155–71

Voll G. 1976. Recrystallization of quartz, biotite, and feldspars from Erstfeld to the Leventina Nappe, Swiss Alps, and its geological significance. *Schweiz. Mineral. Petrog. Mitt.* 56:641–47

Wang K. 2007. Elastic and viscoelastic models of crustal deformation in subduction earthquake cycles. In *The Seismogenic Zone of Subduction Thrust Faults*, ed. TH Dixon, JC Moore, pp. 540–75. New York: Columbia Univ. Press

Warren JM, Hirth G. 2006. Grain size sensitive deformation mechanisms in naturally deformed peridotites. *Earth Planet. Sci. Lett.* 248:438–50

Weber M, Abu-Ayyash K, Abueladas A, Agnon A, Al-Amoush H, et al. 2004. The crustal structure of the Dead Sea Transform. *Geophys. J. Int.* 156:655–81

Wilson CK, Jones CH, Molnar P, Sheehan AF, Boyd OS. 2004. Distributed deformation in the lower crust and upper mantle beneath a continental strike-slip fault zone: Marlborough fault system, South Island, New Zealand. *Geology* 32:837–40

Wittlinger G, Tapponnier P, Poupinet G, Mei J, Danian S, et al. 1998. Tomographic evidence for localized lithospheric shear along the Altyn Tagh fault. *Science* 282:74–76

Wu P. 2002. Effects of mantle flow law stress exponent on postglacial induced surface motion and gravity in Laurentia. *Geophys. J. Int.* 148:676–86

Wu P. 2005. Effects of lateral variations in lithospheric thickness and mantle viscosity on glacially induced surface motion in Laurentia. *Earth Planet. Sci. Lett.* 235:549–63

Zhang S, Karato S-I. 1995. Lattice preferred orientation of olivine aggregates deformed in simple shear. *Nature* 375:774–77

Zhu L. 2000. Crustal structure across the San Andreas fault, southern California from teleseismic converted waves. *Earth Planet. Sci. Lett.* 179:183–90

Zoback MD, Zoback ML, Mount VS, Suppe J, Eaton JP, et al. 1987. New evidence on the state of stress of the San Andreas fault system. *Science* 238:1105–11

Zweck C, Freymueller JT, Cohen SC. 2002. The 1964 great Alaska earthquake: present day and cumulative postseismic deformation in the western Kenai Peninsula. *Phys. Earth Planet. Int.* 132:5–20

Annual Review
of Earth and
Planetary Sciences
Volume 36, 2008

Contents

Frontispiece
Margaret Galland Kivelson xii

The Rest of the Solar System
Margaret Galland Kivelson 1

Abrupt Climate Changes: How Freshening of the Northern Atlantic Affects the Thermohaline and Wind-Driven Oceanic Circulations
Marcelo Barreiro, Alexey Fedorov, Ronald Pacanowski, and S. George Philander 33

Geodynamic Significance of Seismic Anisotropy of the Upper Mantle: New Insights from Laboratory Studies
Shun-ichiro Karato, Haemyeong Jung, Ikuo Katayama, and Philip Skemer 59

The History and Nature of Wind Erosion in Deserts
Andrew S. Goudie 97

Groundwater Age and Groundwater Age Dating
Craig M. Bethke and Thomas M. Johnson 121

Diffusion in Solid Silicates: A Tool to Track Timescales of Processes Comes of Age
Sumit Chakraborty 153

Spacecraft Observations of the Martian Atmosphere
Michael D. Smith 191

Crinoid Ecological Morphology
Tomasz K. Baumiller 221

Oceanic Euxinia in Earth History: Causes and Consequences
Katja M. Meyer and Lee R. Kump 251

The Basement of the Central Andes: The Arequipa and Related Terranes
Victor A. Ramos 289

Modeling the Dynamics of Subducting Slabs
Magali I. Billen 325

Geology and Evolution of the Southern Dead Sea Fault with Emphasis on Subsurface Structure
Zvi Ben-Avraham, Zvi Garfunkel, and Michael Lazar 357

The Redox State of Earth's Mantle
Daniel J. Frost and Catherine A. McCammon 389

The Seismic Structure and Dynamics of the Mantle Wedge
Douglas A. Wiens, James A. Conder, and Ulrich H. Faul 421

The Iron Isotope Fingerprints of Redox and Biogeochemical Cycling in the Modern and Ancient Earth
Clark M. Johnson, Brian L. Beard, and Eric E. Roden 457

The Cordilleran Ribbon Continent of North America
Stephen T. Johnston 495

Rheology of the Lower Crust and Upper Mantle: Evidence from Rock Mechanics, Geodesy, and Field Observations
Roland Bürgmann and Georg Dresen 531

The Postperovskite Transition
Sang-Heon Shim 569

Coastal Impacts Due to Sea-Level Rise
Duncan M. FitzGerald, Michael S. Fenster, Britt A. Argow, and Ilya V. Buynevich 601

Indexes

Cumulative Index of Contributing Authors, Volumes 26–36 649

Cumulative Index of Chapter Titles, Volumes 26–36 653

Errata

An online log of corrections to *Annual Review of Earth and Planetary Sciences* articles may be found at http://earth.annualreviews.org

SUPPLEMENTAL TABLE 1 Experimental flow law parameters $\dot{\varepsilon} = A\sigma^n d^{-m} f_{H_2O}^r e^{-\frac{(Q+pV)}{RT}}$

Rock	logA ($MPa^{-n}\mu m^m s^{-1}$)	n	Q (kJ/mol)	m	r	V (cm^3/mol)	Reference
Olivine							
olivine (wet)	4.7	1±0.2	295	3.0	1	20	(Mei & Kohlstedt 2000a)
olivine (wet)	7.4	1	375±75	3	1	20	(Hirth & Kohlstedt 2003)
olivine (dry)	9.2	1	375±50	3	-	10	(Hirth & Kohlstedt 2003)
olivine (dry)	10.3±0.5	1.4±0.1	484±30	3.0	-	-	(Faul & Jackson 2006)
olivine (wet)	3.2	3±0.1	470±40	0.0	0.98	20	(Mei & Kohlstedt 2000b)
olivine (dry)	6.1±0.2	3±0.1	510±30	0.0	0.0	14±2	(Karato & Jung 2003)
olivine (wet)	2.9±0.1	3±0.1	470±40	0.0	1.2±0.1	24±3	(Karato & Jung 2003)
olivine (wet)	3.2	3.5±0.3	520±40	0.0	1.2±0.4	22±11	(Hirth & Kohlstedt 2003)
olivine (dry)	5.0	3.5±0.3	530±4	0.0	-	18	(Hirth & Kohlstedt 2003)
Pyroxene							
cpx (dry)	25.3±0.8	1	760±20	3.0	-	-	(Hier-Majumder et al 2005)
cpx (wet)	7.9±1.0	1	340±30	3.0	1.4±0.2	14±6	(Hier-Majumder et al 2005)
cpx (dry)	15.1±0.7	1	560±30	3.0	-	-	(Bystricky & Mackwell 2001)
diopside (dry)	14±1.5	1	528±42	3.0	-	-	(Dimanov & Dresen 2005)
diopside (wet)	8.1±0.4	1	337±25	3.0	-	-	(Dimanov & Dresen 2005)
cpx (wet)	6.7±0.1	2.7±0.3	670±40	0.0	3±0.6	0.0	(Chen et al 2006)
cpx (dry)	9.8±0.5	4.7±0.2	760±40	0.0	-	-	(Bystricky & Mackwell 2001)
cpx (dry)	10.8±0.9	4.7	760	0.0	-	-	(Bystricky & Mackwell 2001)
diopside (dry)	5.3±1.8	5.5±0.1	691±46	0.0	-	-	(Dimanov & Dresen 2005)
diopside (wet)	0.8±1.3	5.5±0.1	534±32	0.0	-	-	(Dimanov & Dresen 2005)
omphacite (wet)	-2	3.5±0.2	310±50	0.0	-	-	(Zhang et al 2006)
jadeite (wet)	-3.3 ± 2.0	3.7±0.4	326±27	0.0	-	-	(Orzol et al 2006)
Feldspar							
anorthite (dry)	12.1±0.6	1±0.1	467±16	3.0	-	-	(Rybacki & Dresen 2000)
anorthite (wet)	1.7±0.2	1±0.1	170±6	3.0	-	-	(Rybacki & Dresen 2000)
anorthite (dry)	12.1	1	460	3.0	0.0	24±21	(Rybacki et al 2006)
anorthite (wet)	-0.7	1	159	3.0	1±0.3	38±21	(Rybacki et al 2006)
anorthite (dry)	12.7±0.8	3±0.4	648±20	0.0	-	-	(Rybacki & Dresen 2000)
anorthite (wet)	2.6±0.3	3±0.2	356±9	0.0	-	-	(Rybacki & Dresen 2000)
anorthite (dry)	12.7	3	641	0.0	0.0	24	(Rybacki et al 2006)
anorthite (wet)	0.2	3	345	0.0	1	38	(Rybacki et al 2006)
Quartz							
qtz (wet)	-0.4±2.1	1±0.1	220±55	2±0.8	-	-	(Rutter & Brodie 2004a)
qtz (wet)	-4.9±0.4	3±0.2	242±24	0.0	1	-	(Rutter & Brodie 2004b)

qtz (wet)	-11.2±0.6	4	135±15	0.0	1	-	(Hirth et al 2001)

[a] Experiments with exponent n ≈ 1 indicate dominant diffusion creep; n = 2-6 deform in dislocation creep regime.

TABLE REFERENCES

Bystricky M, Mackwell S. 2001. Creep of dry clinopyroxenite aggregates. *J. Geophys. Res.* 106: 13443-54

Chen S, Hiraga K, Kohlstedt DL. 2006. Water weakening of clinopyroxene in the dislocation creep regime. *J. Geophys. Res.* 111: doi:10.1029/2005JB003885

Dimanov A, Dresen G. 2005. Rheology of synthetic anorthite-diopside aggregates: Implications for ductile shear zones. *J. Geophys. Res.* 110: doi:10.1029/2004JB003431

Faul U, Jackson I. 2007. Diffusion creep of dry melt-free olivine. *J. Geophys. Res.* 112: doi:10.1029/2006JB004586

Hier-Majumder S, Mei S, Kohlstedt DL. 2005. Water weakening in clinopyroxene in diffusion creep. *J. Geophys. Res.* 110: doi:10.1029/2004JB003414

Hirth G, Kohlstedt DL. 2003. Rheology of the upper mantle and the mantle wedge: A view from the experimentalists. In *Inside the subduction factory*, ed. J Eiler, pp. 83-105: American Geophysical Union Monograph

Hirth G, Teyssier C, Dunlap WJ. 2001. An evaluation of quartzite flow laws based on comparisons between experimentally and naturally deformed rocks. *Int. J. Earth Sci.* 90: 77-87

Karato S-I, Jung H. 2003. Effects of pressure on high-temperature dislocation creep in olivine. *Philosoph. Mag.* 83: 401-14

Mei S, Kohlstedt DL. 2000a. Influence of water on plastic deformation of olivine aggregates 1. Diffusion creep regime. *J. Geophys. Res.* 105: 21457-69

Mei S, Kohlstedt DL. 2000b. Influence of water on plastic deformation of olivine aggregates 2. Dislocation creep regime. *J. Geophys. Res.* 105: 21471-81

Orzol J, Stöckhert B, Trepmann CA, Rummel F. 2006. Experimental deformation of synthetic wet jadeite aggregates. *J. Geophys. Res.* 111: doi10.1029/2005JB003706

Rutter EH, Brodie KH. 2004a. Experimental grain size-sensitive flow of hot-pressed Brazilian quartz aggregates. *J. Struct. Geol.* 26: 2011-23

Rutter EH, Brodie KH. 2004b. Experimental intracrystalline plastic flow in hot-pressed synthetic quartzite prepared from Brazilian quartz crystals. *J. Struct. Geol.* 26: 259-70

Rybacki E, Dresen G. 2000. Dislocation and diffusion creep of synthetic anorthite aggregates. *J. Geophys. Res.* 105: 26017-36

Rybacki E, Gottschalk M, Wirth R, Dresen G. 2006. Influence of water fugacity and activation volume on the flow properties of fine-grained anorthite aggregates. *J. Geophys. Res.* 111: doi:10.1029/2005JB003663

Zhang J, Green HW, Bozhilov KN. 2006. Rheology of omphacite at high temperature and pressure and significance of its lattice preferred orientation. *Earth Planet. Sci. Lett.* 246: 432-443

SUPPLEMENTAL TABLE 2 Viscosity estimates derived from geodetic measurements of post-loading deformation[a]

Source event	Mw	Slip[b]	Tectonics[c]	Viscosity (x 10^{18} Pa s)		Reference
				LC	UM	
Earthquakes						
1915-54 Central Nevada	7.6	ss/ns	C-PBZ/BA	> 100	1-7	(Gourmelen & Amelung 2005)
1915-54 Central Nevada	7.6	ss/ns	C-PBZ/BA	100-300	10-30	(Hammond et al 2007)
1959 Hebken Lake,		ns	C-PBZ/BA	> 100	4	(Nishimura & Thatcher 2003)
1992 Landers[d]	7.4	ss	C-PBZ/BA	8-24	1-6	(Pollitz et al 2000)
1997 Manyi, Tibet	7.6	ss	C-PBZ	4-8	-	(Ryder et al 2007)
1999 Hector Mine[d]	7.1	ss	C-PBZ/BA	32	4.6	(Pollitz 2003)
1999 Izmit, Turkey	7.4	ss	C-PBZ	20-50	20-50	Hearn et al., 2007 unpublished
2000 South Iceland	6.5	ss	MOR-PBZ	10	3	(Árnadóttir et al 2005)
2002 Denali[d]	7.8	ss	C-PBZ/BA	> 10	2-4	(Freed et al 2006)
Global subduction events	≤9.5	ts	PBZ/BA	-	~10	Table 1 of (Wang 2007)
Lake Level Fluctuations						
Lake Bonneville			C-PBZ/BA	1000	0.5-5	(Bills et al 1994)
Lake Lahontan			C-PBZ/BA	>800	0.5-5	(Bills et al 2007)
Lake Meade Reservoir			C-PBZ/BA	> 40	1	(Cavalié et al 2007, Kaufmann & Amelung 2000)
Glacial unloading						
Fennoscandia			Craton	-	500-1000	(Milne et al 2001)
North America			Craton	-	300-1000	(Tamisiea et al 2007)
Iceland			MOR-PBZ	-	< 10	(Sigmundsson 1991)
Puget Sound			PBZ/BA	-	5-50	(James et al 2000)
Glacier Bay, Alaska			C-PBZ/BA	-	2.5-4	(Larsen et al 2005)
Vatnajokull, Iceland			MOR-PBZ	-	4-10	(Pagli et al 2007)

[a]We consider selected studies that provide constraints on viscous response in the lower crust and/or upper mantle.

[b]ss, strike-slip; ns, normal slip; ts, thrust slip.

[c]C-PBZ, contintental plate boundary zone; MOR-PBZ, Mid ocean ridge plate boundary zone; S-PBZ, subduction plate boundary zone; BA, backarc or former backarc region; craton, continental interior with ~100-km-thick nominally elastic lithosphere.

[d]Both the Mojave Desert and Alaska appear to have a ~10-20-km thin, viscously stronger uppermost mantle layer. Effective viscosities decayed by about an order of magnitude to the listed values at greater depth after about one year.

TABLE REFERENCES

Árnadóttir T, Jónsson S, Pollitz FF, Jiang W, Feigl KL. 2005. Postseismic deformation following the June 2000 earthquake sequence in the south Iceland seismic zone. *J. Geophys. Res.* 110: doi:10.1029/2005JB003701

Bills BG, Adams KD, Wesnousky SG. 2007. Viscosity structure of the crust and upper mantle in western Nevada from isostatic rebound patterns of Lake Lahontan shorelines. *J. Geophys. Res.* 112: doi:10.1029/2005JB003941

Bills BG, Currey DR, Marshall GA. 1994. Viscosity estimates for the crust and upper mantle from patterns of lacustrine shoreline deformation in the Eastern Great Basin. *J. Geophys. Res.* 99: 22059-86

Cavalié O, Doin M-P, Lasserre C, Briole P. 2007. Ground motion measurement in the Lake Mead area, Nevada, by differential synthetic aperture radar interferometry time series analysis: Probing the lithosphere rheological structure. *J. Geophys. Res.* 112: doi:10.1029/2006JB004344

Freed AM, Bürgmann R, Calais E, Freymueller JT, Hreinsdóttir S. 2006. Implications of deformation following the 2002 Denali, Alaska earthquake for postseismic relaxation processes and lithospheric rheology. *J. Geophys. Res.* 111: doi:10.1029/2005JB003894

Gourmelen, Amelung F. 2005. Postseismic mantle relaxation in the Central Nevada Seismic Belt. *Science* 310: 1473-6

Hammond WC, Kreemer C, Blewitt G. 2007. Geodetic constraints on contemporary deformation in the northern Walker Lane: 3, Central Nevada Seismic Belt postseismic relaxation. *Geol. Soc. Am. Bull.*

James TS, Clague JJ, Wang K, Hutchinson I. 2000. Postglacial rebound at the northern Cascadia subduction zone. *Quat. Sci. Rev.* 19: 1527-41

Kaufmann G, Amelung F. 2000. Reservoir-induced deformation and continental rheology in the vicinity of Lake Mead, Nevada. *J. Geophys. Res.* 105: 16341-58

Larsen CF, Motyka RJ, Freymueller JT, Echelmeyer KA, Ivins ER. 2005. Rapid viscoelastic uplift in southeast Alaska caused by post-Little Ice Age glacial retreat. *Earth Planet. Sci. Lett.* 237: 548-60

Milne GA, Davis JL, Mitrovica JX, Scherneck H-G, Johansson JM, et al. 2001. Space-geodetic constraints on glacial isostatic adjustment in Fennoscandia. *Science* 291: 2381-5

Nishimura T, Thatcher W. 2003. Rheology of the lithosphere inferred from postseismic uplift following the 1959 Hebgen Lake earthquake. *J. Geophys. Res.* 108: doi:10.1029/2002JB002191

Pagli C, Sigmundsson F, Lund B, Sturkell E, Geirson H, et al. 2007. Glacio-istostatic deformation around the Vatnajökull ice cap, Iceland, induced by recent climate warming: GPS observations and finite element modeling. *J. Geophys. Res.* 112: doi:10.1029/2006JB004421

Pollitz F. 2003. Transient rheology of the uppermost mantle beneath the Mojave Desert, California. *Earth Planet. Sci. Lett.* 215: 89-104

Pollitz FF, Peltzer G, Bürgmann R. 2000. Mobility of continental mantle: Evidence from postseismic geodetic observations following the 1992 Landers earthquake. *J. Geophys. Res.* 105: 8035-54

Ryder I, Parsons BE, Wright TJ, Funning GJ. 2007. Postseismic motion following the 1997 Manyi (Tibet) earthquake: InSAR observations and modeling. *Geophys. J. Int.*: doi: 10.1111/j.365-246X.2006.03312.x

Sigmundsson F. 1991. Post-glacial rebound and asthenosphere viscosity in Iceland. *Geophys. Res. Lett.* 18: 1131-4

Tamisiea ME, Mitrovica JX, Davis JL. 2007. GRACE gravity data constrain ancient ice geometries and continental dynamics over Laurentia. *Science* 316: 881-3

Wang K. 2007. Elastic and viscoelastic models of crustal deformation in subduction earthquake cycles. In *The Seismogenic Zone of Subduction Thrust Faults*, ed. TH Dixon, JC Moore, New York: Columbia University Press

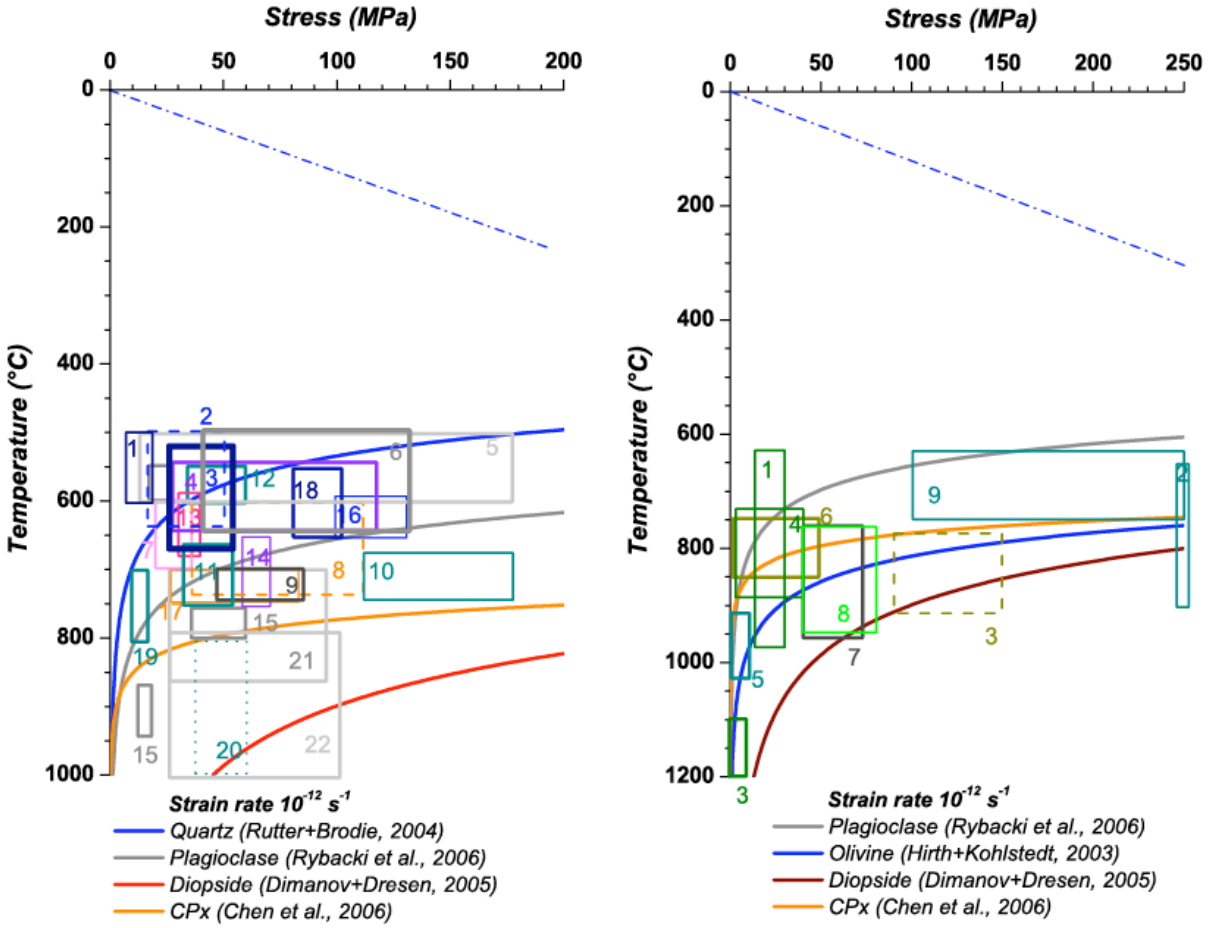

Figure 7 Paleostress estimates from mylonite shear zones transecting lower crust (left) and upper mantle (right). Each box represents stress-temperature estimates for a particular shear zone. A list with all numbered references is provided below. Stress estimates are mostly based on the inverse relation between recrystallized grain size and flow stress (Twiss, 1977; Van der Wal et al., 1993). Graphs indicate extrapolated laboratory data for dislocation creep of rocks at hydrous conditions. The field data from lower crustal shear zones are bracketed by the flow strength of quartzite and pyroxenite. Paleostress estimates from upper mantle shear zones are bracketed by flow strength of anorthosite and pyroxenite. The field estimates cluster between about 10 and 50 MPa in lower crust and upper mantle shear zones. However, paleostresses could be severely overestimated, if deformation in shear zones is dominated by diffusion-controlled creep.

REFERENCES OF PALEOSTRESS ESTIMATES IN FIGURE 7

Left panel: Lower crust:

1.) Stipp, M., Stünitz, H., Heilbronner, R., Schmid, S. M., 2002. Dynamic recrystallization of quartz: correlation between natural and experimental conditions, *Geol. Soc. London Spec. Pub.*, 200: 171-190

2.) Zulauf, G., 2001. Structural style, deformation mechanisms and paleodifferential stress along an exposed crustal section: constraints on the rheology of quartzofeldspathic

rocks at supra- and infrastructural levels (Bohemian Massif), *Tectonophys*., 332: 211-237

3.) Fliervoet, T.F., White, S.H., Drury, M.R., 1997. Evidence for dominant grain-boundary sliding deformation in greenschist- and amphibolite-grade ploymineralic ultramylonites from the Redbank Deformed Zone, Central Australia, *J. Struct. Geol*., 19: 1495-1520

4.) Behrmann, J. H., Mainprice, D., 1987. Deformation mechanisms in a high-temperature quartz-feldspar mylonite: evidence for superplastic flow in the lower continental crust, *Tectonophys.,* 140: 297-305

5.) Steffen, K., Selverstone, J., Brearley, A., 2001. Episodic weakening and strengthening during synmetamorphic deformation in a deep-crustal shear zone in the Alps, *Geol. Soc. London Spec. Pub*., 186: 141-156

6.) Kenkmann, T., Dresen, G., 2002. Dislocation microstructures and phase distribution in a lower crustal shear zone - an example from the Ivrea-Zone, Italy, *Int. J. Earth Sci*., 91: 445-458

7.) Lapworth, T., Wheeler, J., Prior, D. J., 2002. The deformation of plagioclase investigated using electron backscatter diffraction crystallographic preferred orientation data, *J. Struct. Geol*., 24: 387-399

8.) Ji, S., Mainprice, D., 1990. Recrystallisation and fabric development in plagioclase, *Geology*, 98: 65-79

9.) Kruse, R., Stünitz, H., 1999. Deformation mechanisms and phase distribution in mafic high-temperature mylonites from the Jotun Nappe, southern Norway, *Tectonophys*., 303: 223-249

10.) Altenberger, U., Wilhelm, S., 2000. Ductile deformation of K-feldspar in dry eclogite facies shear zones in the Bergen Arcs, Norway, *Tectonophys*., 320: 107-121

11.) Hippertt, J., Rocha, A., Lana, C., Egydio-Silva, M., Takeshita, T., 2001. Quartz plastic segregation and ribbon development in high-grade striped gneisses, *J. Struct. Geol*., 23: 67-80

12.) Schulmann, K., Mlcoch, B., Melka, R., 1996. High-temperature microstructures and rheology of deformed granite, Erzgebirge, Bohemian Massif, *J. Struct. Geol*., 18, 6: 719-733

13.) Rosenberg, C. L., Stünitz, H., 2003. Deformation and recrystallization of plagioclase along a temperature gradient: an example from the Bergell tonalite, *J. Struct. Geol*., 25: 389-408

14.) Gower, R. J. W., Simpson, C., 1992. Phase boundary mobility in naturally deformed, high-grade quartzofeldspathic rocks: evidence for diffusional creep, *J. Struct. Geol*., 14, 3: 301-313

15.) Lafrance, B., John, B. E., Frost, B. R., 1998. Ultra high-temperature and subsolidus shear zones: examples from the Poe Mountain anorthosite, Wyoming, *J. Struct. Geol*., 20, 7: 945-955

16.) Vauchez, A., 1987. The development of discrete shear-zones in a granite: stress, strain and changes in deformation mechanisms, *Tectonophys.,* 133: 137-156

17.) Egydio-Silva, M., Vauchez, A., Bascou, J., Hippertt, J., 2002. High-temperature deformation in the Neoproterozoic transpressional Ribeira belt, southeast Brazil, *Tectonophys*., 352: 203-224

18.) Christie, J. M., Ord, A., 1980. Flow stress from microstructures of mylonites: example and current assessment, *J .Geophys. Res*., 85, B11: 6253-6262

19.) Martelat, J. E., Schulmann, K., Lardeaux, J. M., Nicollet, C., Cardon, H., Granulite microfabrics and deformation mechanisms in southern Madagascar, *J. Struct. Geol*., 21: 671-687

20.) Hanmer, Simon K., 2000. Matrix mosaics, brittle deformation, and elongate porphyroclasts: granulite facies microstructures in the Striding - Athabasca mylonite zone, western Canada, *J. Struct. Geol.*, 22: 947-967
21.) White, Joseph C., 2004. Instability and localization of deformation in lower crust granulites, Minas fault zone, Nova Scotia, Canada, *Geol. Soc. London Spec. Pub.*, 224: 25-37
22.) Mehl, L., Hirth G., 2008. Plagioclase recrystallization and preferred orientation in layered mylonites: Evaluation of flow laws for the lower crust, JGR, in press

Right panel: mantle

1.) Skemer, P., Katayama, I., Karato, S.-I., 2006. Deformation fabrics of the Cima di Gagnone peridotite massif, Central Alps, Switzerland: evidence of deformation at low temperatures in the presence of water, *Contrib. Mineral. Petrol.* 152: 43-51, doi: 10.1007/s00410-006-0093-4
2.) Vissers, R.L.M., Drury M.R., Newman J., Fliervoet T.F., 1997. Mylonitic deformation in upper mantle peridotites of the North Pyrenean Zone (France): implications for strength and strain localization in the lithosphere, *Tectonophys.*, 279: 303-325
3.) Drury, M.R., Vissers, R.L.M., Van der Wal., D., Hoogerduijn Strating, E. H. , 1991. Shear Localisation in Upper Mantle Peridotites, *Pageoph,* 137, 4: 439-460
4.) Dijkstra, A.H., Drury, M.R., Vissers, R.L.M., Newman, J., 2002. On the role of melt-rock reaction in mantle shear zone formation in the Othris Peridotite Massif (Greece), *J. Struct. Geol.*, 24: 1431-1450
5.) Vissers, R.L.M., Drury, M.R., Hoogerduijn Strating, E.H., Spiers, C.J., Van der Wal, D. 1995. Mantle shear zones and their effect on lithosphere strength during continental breakup. *Tectonophys.* 249: 155-71
6.) Newman J, Lamb, W.M., Drury, M.R., Vissers, R.L.M., 1999. Deformation processes in a peridotite shear zone: reaction-softening by an H_2O-deficient, continuous net transfer reaction. *Tectonophys.* 303: 193–222
7.) Furusho, M., Kanagawa, K., 1999. Transformation-induced strain localization in a lherzolite mylonite from the Hidaka metamorphic belt of central Hokkaido, Japan, *Tectonophys.* 313: 411-432
8.) Jin, D., Karato, S., Obata, M., 1998. Mechanisms of shear localization in the continental lithosphere: inference from the deformation microstructures of peridotites from the Ivrea zone, northwestern Italy, *J. Struct. Geol.*, 20: 195-209
9.) Warren, J.M., Hirth, G.,2006. Grain size sensitive deformation mechanisms in naturally deformed peridotites. *Earth Planet. Sci. Lett.* 248: 438-50